Further icing experiments on an unheated non-rotating cylinder

Stallabrass, J. R.; Hearty, Patrick F.

Laboratory Technical Report (National Research Council of Canada. Division of Mechanical Engineering. Low Temperature); no. LTR-LT-105, 1979-11

National Research Council Canada
Conseil national de recherches Canada

DIVISION OF MECHANICAL ENGINEERING

DIVISION DE GÉNIE MÉCANIQUE

PAGES
PAGES 27

FIG.
DIAG. 32

TABLES
TABLES 6

REPORT
RAPPORT

LABORATORY / LABORATOIRE

Low Temperature

REPORT
RAPPORT LTR-LT-105

DATE
DATE November 1979

LAB. ORDER
COMM. LAB. L.O. 16329A

FILE
DOSSIER 3741-2

FOR
POUR Internal

REFERENCE
RÉFÉRENCE

LTR - LT - 105

FURTHER ICING EXPERIMENTS ON AN UNHEATED NON-ROTATING CYLINDER

SUBMITTED BY
PRÉSENTÉ PAR T. R. Ringer
LABORATORY HEAD
CHEF DE LABORATOIRE

AUTHOR
AUTEUR J. R. Stallabrass
P. F. Hearty

APPROVED
APPROUVÉ D. C. MacPhail
DIRECTOR
DIRECTEUR

COPY NO.
COPIE NR. 2

TABLE OF CONTENTS

		Page
	LIST OF ILLUSTRATIONS	5
	SUMMARY	7
1.0	INTRODUCTION	9
2.0	EXPERIMENTAL EQUIPMENT	9
	2.1 The Cylinder	9
	2.2 Ice Particle Nozzle	10
3.0	EXPERIMENTAL PROCEDURES	11
4.0	TEST RESULTS AND DISCUSSION	12
	4.1 Dry Air Measurements	12
	4.2 Icing Characteristics	12
	4.2.1 Morphological Aspects	12
	4.2.2 Temperature Measurements	16
5.0	CONCLUSIONS	20
6.0	REFERENCES	20
	TABLE I - SUMMARY OF TEST CONDITIONS AND ICING RESULTS AT A NOMINAL AIR TEMPERATURE OF -15°C	22
	TABLE II - SUMMARY OF TEST CONDITIONS AND ICING RESULTS AT A NOMINAL AIR TEMPERATURE OF -5°C	23
	TABLE III - EFFECT OF ICE PARTICLES ON THE EQUIVALENT LIQUID WATER CONTENT DERIVED BY THE ROTATING CYLINDER METHOD	24
	TABLE IV - NUCLEATION DELAY TIMES FOR LIQUID ONLY TESTS	25
	TABLE V - MEASURED ICING TEMPERATURES AROUND CYLINDER FOR TESTS WITH LIQUID WATER ONLY	26
	TABLE VI - MEASURED ICING TEMPERATURES AROUND CYLINDER FOR TESTS IN MIXED CONDITIONS	27
	ILLUSTRATIONS - Figures 1 to 32	

LIST OF ILLUSTRATIONS

	Figure
MK II Snow Nozzle	1
High Speed Icing Wind Tunnel	2
Methods of Recording Ice Profile	3
Dry Air Recovery Temperatures for 0.0254 m Diameter Cylinder	4
Cylinder Icing at -15°C and L.W.C. = 0.4 g/m^3 -- Comparison between Liquid Only and Mixed Conditions	5
Cylinder Icing Profiles at -15°C and L.W.C. = 0.4 g/m^3 -- Comparison between Liquid Only and Mixed Conditions	6
Cylinder Icing at -15°C and L.W.C. = 1.2 g/m^3 -- Comparison between Liquid Only and Mixed Conditions	7
Cylinder Icing Profiles at -15°C and L.W.C. = 1.2 g/m^3 -- Comparison between Liquid Only and Mixed Conditions	8
Cylinder Icing at -5°C and L.W.C. = 0.4 g/m^3 -- Comparison between Liquid Only and Mixed Conditions	9
Cylinder Icing Profiles at -5°C and L.W.C. = 0.4 g/m^3 -- Comparison between Liquid Only and Mixed Conditions	10
Cylinder Icing at -5°C and L.W.C. = 0.4 g/m^3 -- Comparison between Liquid Only and Mixed Conditions	11
Cylinder Icing Profiles at -5°C and L.W.C. = 1.2 g/m^3 -- Comparison between Liquid Only and Mixed Conditions	12
Stagnation Line Icing Rate at -15°C and L.W.C. of 1.2 g/m^3, Liquid Only	13
Stagnation Line Icing Rate at -15°C and L.W.C. of 0.4 g/m^3, Liquid Only	14
Stagnation Line Icing Rate at -5°C, Liquid Only	15
Comparison of Ice Profiles obtained in Present Tests with Those of Ref. 1 for Corresponding Mixed Icing Conditions	16
Stagnation Line Icing Rate in Mixed Conditions at -15°C	17
Stagnation Line Icing Rate in Mixed Conditions at -5°C	18
Cylinder Ice Accretion Rate as a Function of Velocity at a Temperature of -15°C	19
Cylinder Ice Accretion Rate as a Function of Velocity at a Temperature of -5°C	20
Cylinder Surface Temperature Histories for Initial 20 Seconds of Tests 36 and 37	21
Cylinder Surface Temperature Histories for Initial 20 Seconds of Tests 31 and 32	22

LIST OF ILLUSTRATIONS (cont'd)

	Figure
Cylinder Surface Temperature Histories for Initial 20 Seconds of Tests 25 and 26	23
Cylinder Surface Temperature History for Initial 30 Seconds of Test 21	24
Cylinder Surface Temperature Histories for Initial 20 Seconds of Tests 41 and 42	25
Experimental and Model-Predicted Ice Surface Temperatures around Cylinder at -15°C Air Temperature with 0.4 g/m^3 Liquid Water Only	26
Experimental and Model-Predicted Ice Surface Temperatures around Cylinder at -15°C Air Temperature with 1.2 g/m^3 Liquid Water Only	27
Experimental and Model-Predicted Ice Surface Temperatures around Cylinder at -5°C Air Temperature with Liquid Water Only	28
Experimental and Model-Predicted Ice Surface Temperatures around Cylinder at -15°C Air Temperature under Mixed Conditions with L.W.C. = 0.4 g/m^3	29
Experimental and Model-Predicted Ice Surface Temperatures around Cylinder at -15°C Air Temperature under Mixed Conditions with L.W.C. = 1.2 g/m^3	30
Experimental and Model-Predicted Ice Surface Temperatures around Cylinder at -5°C Air Temperature under Mixed Conditions with L.W.C. = 0.4 g/m^3	31
Experimental and Model-Predicted Ice Surface Temperatures around Cylinder at -5°C Air Temperature under Mixed Conditions with L.W.C. = 1.2 g/m^3	32

SUMMARY

Experiments conducted in an icing wind tunnel on the icing characteristics of a cylinder exposed to mixed icing conditions of supercooled water droplets and "snow" nozzle generated ice particles show that the characteristics differ greatly from those of water droplet only conditions or from those of mixed conditions using natural snow crystals for the ice phase.

Surface temperature measurements on the frontal part of the cylinder confirm in the dry growth regime of ice accretion the validity of a mathematical model of cylinder icing developed earlier, and shed some insight into the change in convective heat transfer that occurs with increasing wetness in the wet growth regime. Also confirmed is the existence of a nucleation delay at the start of an icing encounter, this delay being shown to occur at low water impingement rates and with total air temperatures approaching the melting point.

1.0 INTRODUCTION

Icing wind tunnel studies of the icing characteristics of a cylinder in clouds of supercooled water droplets and in mixed clouds of supercooled water droplets and ice (snow) crystals were reported in Ref. 1. The ice phase particles used in that series of tests were natural snow crystals, collected in as freshly fallen a state as possible, and injected into the icing wind tunnel. Such a technique is possible only in locations, such as Ottawa, where a significant number of snowfalls are experienced throughout the winter. Elsewhere a number of facilities have resorted to the use of ice crystal nozzles to simulate atmospheric ice particles. Such "snow" is a poor simulation of natural atmospheric ice crystals, but in view of its use in mixed icing tests it was considered advisable to repeat the tests reported in Ref. 1 but using the product of an ice crystal nozzle instead of natural snow crystals.

This report therefore presents the results of mixed icing tests on a cylinder using a "snow" nozzle to produce the ice phase. In addition, temperature measurements were made at four angular locations around the cylinder surface, and so provide a more sensitive and reliable check of the numerical icing model presented in Ref. 1.

2.0 EXPERIMENTAL EQUIPMENT

The experiments described were performed on a 0.0254 m diameter cylinder in the high speed icing tunnel at the Low Temperature Laboratory, National Research Council. With the exception of the cylinder and the method of producing mixed conditions in the wind tunnel, the experimental equipment was the same as that used previously and described in Ref. 1. Only those areas of difference will be described here.

2.1 The Cylinder

The cylinder differed from that used for the experiments described in Ref. 1 in being made of wood (yellow birch). The thermal properties of yellow birch are variously given as:- thermal conductivity 0.14 W/mK, specific heat 1.1 x 10^3 J/kgK, and specific gravity 0.69 at a moisture content of 12% (Ref. 2) or thermal conductivity 0.18 W/mK, and specific gravity 0.64 at a moisture content of 10.8% (Ref. 3). Thus both the thermal conductivity and the specific gravity may be assumed to be about one half of those for the bakelite cylinder used in the earlier tests (Ref. 1). The specific heat is only slightly less than that of bakelite.

Four flat-strip copper/constantan thermocouples, 0.8 mm wide and 0.05 mm thick, were bonded longitudinally to the surface of the cylinder with their junctions at the mid-length of the cylinder. Angular locations of the junctions around the cylinder, measured from stagnation, were -15°, 0°, +30°, and +60°. The flat copper and constantan strips were run the complete length of the cylinder. The cylinder surface was built up flush with the strip thermocouples by successive coats of black enamel paint, rubbed smooth at

each coat. About 12 coats were required until no discontinuity was noticeable at the strips.

The cylinder was mounted in the wind tunnel in the same manner as described for the bakelite cylinder in Ref. 1.

A C.E.C. optical strip chart recorder was used to record the output of the thermocouples using C.E.C. Type 241 galvanometers. Reference voltage was provided by a Kaye Ice-Point Reference Standard, Model 2150-4. A calibration of deflection vs. temperature was made for each of the thermocouple/galvanometer combinations by immersing the cylinder in an oil bath and allowing the temperature to stabilize, first at room temperature and then at four sub-zero temperatures in a cold box. The temperature of the oil bath was monitored by measuring the resistance of a calibrated thermistor. Regression analysis provided the following 2nd order fits for the thermocouples at the indicated angular locations:-

@ -15°	$T = -0.0290 + 11.1711D - 0.3360D^2$
@ 0°	$T = -0.0441 + 12.1328D - 0.2042D^2$
@ +30°	$T = -0.0549 + 11.6040D - 0.1286D^2$
@ +60°	$T = 0.0674 + 11.2757D - 0.1843D^2$

where D is the deflection from the galvanometer null position in inches (the strip chart was graduated in inches and tenths of inches), and T is the temperature in °C.

2.2 Ice Particle Nozzle

Ice particles were generated by use of a single nozzle, the configuration of which is shown in Fig. 1 at actual size. Such "snow" nozzles produce small frozen water droplets rather than crystals having hexagonal symmetry characteristics of natural atmospheric snow or ice crystals. Snow nozzles are designed to promote the maximum cooling of the air as it expands through the nozzle, unlike nozzles used for producing the supercooled droplet spray where it is desired to minimize temperature drop. The air not only "atomizes" the water injected through the central tube, but also cools the drops so produced. Should the cooling be sufficient, the water drops will nucleate spontaneously, and subsequent heat loss will complete the freezing of the drops. It is possible that in the expanding air, small ice crystals are formed as a result of the condensation of water vapour from the air, and that these in turn assist in the nucleation of the water spray. Whatever the mechanism, the high air pressures required to cause adequate cooling also result in small particle sizes; reduction in air pressure to produce larger particles results in incomplete freeze-out. This is undesirable in wind tunnel work where flight times of the particles are fractions of a second, but is acceptable for such purposes as snow making on ski slopes where flight times of many seconds permit additional freezing by virtue of convective and evaporative heat losses.

The snow nozzle was located on the centre line of the wind tunnel as far upstream as possible to give maximum flight time to the particles, as shown

in Fig. 2. Air was supplied at room temperature at gauge pressures of up to 650 kPa, while the water was cooled close to 0°C by a heat exchanger immersed in an ice/water bath. Water flow rates of up to 6.8 g/s were used.

Calibration of the nozzle was performed at above freezing temperatures using a Johnson-Williams Liquid Water Content Meter. It was found that air pressure variation had no significant influence on the water content in the test section, but did, as expected, modify the droplet size. The droplet size (median volume diameter) ranged from about 10 μm to about 20 μm depending on the ratio of water flow rate to air pressure.

During actual mixed condition tests, the air pressure was set as low as possible consistent with complete freezing of the particles under the conditions of the test. Because the snow nozzle was situated in the tunnel settling chamber, it was in an ambient air whose temperature was the test total temperature; thus for tests at -5°C the nozzle was in a -0.8°C environment for a velocity of 91.5 m/s and +2.5°C for tests at 122 m/s. Under the 91.5 m/s condition freeze-out was probably marginally complete, while at 122 m/s complete freeze-out was clearly not achieved, although it was not possible to assess its extent.

For most tests the median volume diameter of the ice particles was about 15 μm.

3.0 EXPERIMENTAL PROCEDURES

The same general experimental procedures as used in the earlier series of tests and described in Ref. 1 were again employed. Conditions were chosen to match as nearly as possible those of the earlier mixed condition tests, thus tests were made at working section static temperatures of -5°C and -15°C, at nominal liquid water contents of 0.4 and 1.2 g/m^3 having droplet median volume diameter of approximately 20 μm in both cases, and at airstream velocities of 30.5, 61, 91.5 and 122 m/s. The ice crystal contents used were also chosen to approximate those of the corresponding mixed icing tests of the earlier series.

About 10 seconds prior to each test the strip chart recorder was turned on to provide dry air temperature readings as a base line for the subsequent icing temperatures. About one minute of the icing run was recorded, since beyond this time the thermocouples were becoming significantly insulated by the ice and no longer effectively measured the ice surface temperature.

As before, at the completion of a test run, the tunnel was stopped (and cooled if necessary to prevent melting of the accretion) and measurements were made of the stagnation line ice thickness and that of the horns if appropriate. Photographs were made of the accretion on the cylinder, and its shape was recorded where possible by two methods; the first (which was not possible if the accretion was significantly wider than the cylinder diameter) was by means of a plasticene mould which was subsequently photographed, and the second was to section the accretion at the cylinder mid-span and to remove the ice from the near half of the cylinder. The sectioned ice was then photographed at a shallow angle to the cylinder leading edge. Figure 3 shows a typical example of these two methods of recording the accretion profile. Finally, by optical projection

of these two profiles a composite line drawing of the ice shape was produced (see Figs. 6, 8, 10 and 12), and from this sketch the cross-sectional area of the accretion was measured.

4.0 TEST RESULTS AND DISCUSSION

Table I is a summary of the test conditions and ice accretion measurements for both water only and mixed conditions at a nominal static air temperature of -15°C. A similar summary for a nominal air temperature of -5°C is presented in Table II.

4.1 Dry Air Measurements

Analysis of the temperature recorder traces obtained prior to turning on the icing sprays (and, as appropriate, the snow nozzle) provided a series of local recovery temperature readings at four angular positions around the cylinder. The measurements at each angular location of all tests at the same air speed and nominal static temperature were averaged, and are shown in Fig. 4 compared with curves of cylinder surface temperature calculated using the following expression for the variation of recovery factor around a cylinder:

$$r = 0.7 + 0.3 \cos 1.7\theta \qquad (1)$$

The use of this expression in place of that used in Ref. 1 results in a maximum difference in surface temperature of 0.15°C at an angle of 45° at the maximum air speed (122 m/s) used in these tests.

Fig. 4 demonstrates good agreement between the measured angular variation of temperature and that predicted using expression (1); however, it also demonstrates that the actual tunnel air temperature deviated somewhat from the nominal air temperature as set on the tunnel temperature controller.

Using, then, the mean difference between the measured dry air surface temperatures and the corresponding calculated temperatures, the actual static air temperature for each test was deduced. These are shown in Tables I and II.

4.2 Icing Characteristics

A summary of the tests performed is presented in Tables I and II. The test results fall into two categories, that relating to the physical dimensions and morphology of the ice accretion, and that relating to the temperature history of the cylinder surface as the ice accretion began to form.

4.2.1 Morphological Aspects

Figures 5, 7, 9 and 11 present oblique photographs which depict the overall physical characteristics of the accretions. Each figure presents tests at the same nominal air temperature and liquid water content and compares directly each mixed condition case with its corresponding liquid only case. In a similar manner, Figures 6, 8, 10 and 12 present line drawings of the cross-sections of the deposits, derived, as described in Section 3.0, from cross-sectional photographs and photographs of the plasticene mould (Fig. 3).

Comparison of these figures with those presented in Ref. 1 shows some slight difference in the appearance and shape of some of the deposits in liquid droplet icing conditions. These differences are probably the result of slight variations in tunnel air temperature and liquid water content; however, little difference in stagnation line icing rate was observed, as indicated in Figs. 13, 14 and 15, which present the stagnation growth rate as a function of velocity.

Trends in the characteristics of the ice accretions with variations of the primary icing parameters have been discussed at some length in Ref. 1, and will not be discussed further here.

In the mixed condition tests, remarkable differences are seen in the ice shape and appearance between these tests and those of Ref. 1. Some selected comparisons are shown in Fig. 16. The most striking characteristic in these tests was the pronounced stagnation line peak that gave many of the accretions a wedge-like profile. These wedge-like profiles are seen to be more accentuated at lower velocities and with greater ice crystal to liquid water ratios. In addition, at low speeds generally, but at all speeds when low liquid water content was associated with low temperature, the appearance of the accreted wedge-shaped ice was very white with a rather soft, granular texture. In all cases, however, the accretions were drier in appearance than the corresponding Ref. 1 case.

In general the wedge-shaped form of ice was very similar to the classic streamline or knife-edge form (Ref. 6) that is characteristic of the final form attained at low temperatures with low liquid water contents, and moderately low air speeds on small collectors. It does seem however that, in these mixed condition tests, this streamline form was attained sooner than would be expected with droplet conditions (see in particular the 30.5 m/s case in Fig. 6), since normally the profile has to progress through an increasingly "elliptical" form before the leading edge is of sufficiently small radius of curvature that the local collection efficiency becomes sufficiently high in this region to promote the streamline form of ice. One might suppose in this present case that some form of impact-sintering process takes place in the region of near normal impingement wherein the small ice particles, rather than bounce off in the manner observed for snow crystals of about 1 mm, tend to stick and result in enhanced growth in this region, while in regions of oblique impingement, i.e. on the flanks of the developing wedge, the ice particles, even when wet, tend to bounce off.

The ice growth rate at the stagnation line in mixed conditions is shown in Fig.17 for tests at -15°C, and in Fig. 18 for tests at -5°C. In both these figures comparison is made with the corresponding results from Ref. 1. At -15°C, the stagnation line growth rate is seen in Fig. 17 to differ little from that resulting when actual snow crystals were used in spite of changes in the ice shape. Only at 122 m/s with a L.W.C. of 1.2 g/m^3 is a significant difference in the rates of icing between the two series of tests evident. These measured rates of icing are also compared in Fig. 17 with predicted results for liquid water only using the mathematical model of Ref. 1. This comparison indicates that the presence of ice crystals, whether large or small, has little

effect on the stagnation line rate of icing at an air temperature of -15°C (see also Figs. 13 & 14).

At -5°C (Fig. 18) on the other hand, a considerable increase in stagnation line ice growth rate is seen to result from the radical changes in the ice shape (i.e. from rather flattened glaze ice to highly peaked rime as in Fig. 16(d) and less flattened, smoother glaze) that occur when the small ice particles of these tests are used instead of actual snow crystals.

It is uncertain whether, in this series of tests, erosion of the ice accretion by impinging ice particles was of much significance in view of the small mass of the particles. The ice particles were about 50 times smaller than the natural snow crystals used earlier, hence their individual mass was about 10^{-5} that of the snow crystals.

At corresponding ice crystal mass contents the number of ice particles present in the air stream would have been about 10^5 times the number of snow crystals in the earlier tests. The effect of such a large number of ice particles (in most cases more than the number of liquid water droplets produced by the spray nozzles) would have been to nucleate a large proportion of the supercooled droplets.

It is to be expected that the final cloud would consist of particles ranging from all ice to all water. Particles composed wholly of ice would for the most part be particles from the snow nozzle that had not coalesced with water droplets, together with those resulting from collisions between larger ice particles and smaller droplets. At the other end of the scale, droplets composed wholly of water must be only those droplets that had not come in contact with an ice crystal. In between, the whole range of water/ice ratios might be expected within individual drops. The actual composition of the final cloud will depend on a number of factors, including: the initial total masses of ice particles and water droplets generated, the relative numbers and individual sizes of each, the air temperature, the air speed (determining the time available for collisions to take place and for heat loss from nucleated droplets), and the turbulence in the wind tunnel.

As a check on the hypotheses of droplet nucleation and freeze-out, rotating cylinder[4] measurements were made under a variety of conditions, and the weight of ice accreted was converted in the usual way to obtain an "equivalent liquid water content", i.e. that liquid water content that would have resulted in the same mass of ice as was collected on the rotating cylinder in the mixed phase condition. These rotating cylinder measurements are tabulated in Table III, and demonstrate that at low temperatures (about -15°C) the ice accreted on the small (2.5 mm diameter) cylinder in the mixed condition was equal to that resulting from liquid droplets only having a L.W.C. of slightly over 0.5 of the actual L.W.C. used. At -5°C the equivalent liquid water content was reduced to only about 3/4 of the actual liquid water content. These results suggest quite clearly that, rather than increasing the effective water content by adhering to the icing surface, the ice particles do in fact nucleate enough of the supercooled water droplets that a significant number are sufficiently frozen as to take no part in the icing process.

Referring once more to Table III, an increase in nozzle air pressure is seen to increase the degree of freeze-out slightly, either because of the larger number of (smaller) nucleating ice particles, or because the snow nozzle ice particles are themselves more completely frozen. At -15°C the effect of airspeed on degree of freeze-out appears to be negligible.

It must not be thought, however, that an arbitrary equivalent liquid water content based on such rotating cylinder measurements can necessarily be carried across to bodies of other shapes and/or sizes. Reference to the ice accretion rate column in Tables I and II shows a rather more complex state of affairs, although Test No. 49 (Table I) whose L.W.C. was chosen to be about a half that of Test No. 17 in accordance with the rotating cylinder indications, does in fact have an ice accretion rate close to that of Test 17 (bearing in mind the approximate nature of the ice cross-section measurements from which the accretion rates are derived). Also at -15°C the accretion rates of Tests 18, 19 and 20 (Table II) are in good correspondence with the rotating cylinder tests at 61 m/s and -5°C (Table III).

Comparing actual area accretion rates for the mixed tests with the calculated accretion (impingement) rates for the liquid water component as shown in Tables I and II and Figs. 19 and 20, the amount of ice accreted at 30.5 m/s is seen to be about 90% of the calculated amount, which might be interpreted to suggest that none of the ice particles took part in the accretion process, nor did an additional 10% of the water droplets which were completely frozen out as a result of nucleation by the ice particles. In fact the 90% figure is probably too large since the density of the accretions at this speed was judged to be less than the 890 kg/m^3 assumed in the calculated accretion rate.

At an airspeed of 61 m/s the actual accretion dropped to about 70% of that calculated except for the case of high temperature combined with high L.W.C. (Test 48, Table II, Fig. 20(a)) where 100% was approached. Thus, except for Test 48, the effect was of even more frozen droplets.

Only one mixed condition test was made at 91.5 m/s, that being Test 38 at -5°C and L.W.C. of 0.4 g/m^3 (Table II, Fig. 20(b)). Under these conditions, 50% more ice was accreted than was contributed by the water component alone, suggesting that about 20% of the ice crystal content was now incorporated into the ice deposit.

At 122 m/s and -15°C (Fig. 19), the accretion is only 50% of that calculated for a L.W.C. of 0.43 g/m^3, and 75% when the L.W.C. is 1.18 g/m^3, indicating that even at this high speed, flight times were still long enough to ensure complete ice particle freezing and substantial nucleation and freeze-out of the spray droplets.

At -6.3°C and 122 m/s (Test 39, Fig. 20(b)), with a total temperature above freezing (+1.2°C), the thermodynamics were such that a considerable part of the front of the cylinder remained free of ice, although two large horns grew at about $\pm$70° from the stagnation point (Figs. 9 and 10). The quantity of ice accreted was about 35% of the liquid component impinging, but in this case the water was lost more by water blow-off than by ice particles not sticking.

4.2.2 Temperature Measurements

Cylinder surface temperature measurements were made on each run at the stagnation point ($\alpha = 0$), at 15° below stagnation ($\alpha = -15°C$) and at 30° and 60° above stagnation ($\alpha = +30°$ and $+60°$). Because the original temperature recordings were not of sufficient quality for reproducing here, those of several tests have been traced and are presented as Figures 21 through 25. These figures show a small section of dry air run followed by the first 20 or 30 seconds of icing. Shown too are the galvanometer zero positions from which deflections of each of the four traces were measured and converted to temperatures using the relations given in Section 2.1.

The use of the relationship between recovery factor and angle around the cylinder to confirm the validity of the dry air temperature measurements, and thus to determine a more precise air temperature for each test, has been described in Section 4.1.

Frequently at the start of icing in liquid only conditions, a nucleation delay had been visually observed. The temperature records confirm this phenomenon, examples of which are shown in Figs. 21(a), 22(a) and 24, where, as the cylinder is wetted by the supercooled spray droplets, the surface temperature initially drops slightly as a result of evaporative cooling, and subsequently, as nucleation occurs, rises towards the equilibrium icing temperature. Table IV lists the delay times at each of the four thermocouple positions for all of the liquid only tests. These delay times have been measured from spray initiation until the recorder trace again rose to the initial dry air value. More correctly nucleation would have commenced at the point where the temperature began to increase from its minimum (evaporative) value; however, this point was not always easy to determine, and the difference in most cases was not large except perhaps at an angle of 60°.

It is noticeable that, other conditions being the same, the nucleation delay was greater for low water concentration than for high. Also, with one notable exception, the delay decreased as velocity increased. It seems probable therefore that the greater the quantity of water impinging, the greater the probability of heterogeneous nucleation occurring and hence the sooner freezing would likely occur.

The exception noted above is Test 21 (Fig. 24) where, at 91.5 m/s, -4.6°C and 0.4 g/m^3, the nucleation delay at the stagnation point was 11 seconds. A possible explanation of this is contained in the dry air temperatures which were measured as -0.35°C at the stagnation point and -0.4°C, -1.0°C and -2.2°C at angles of 15°, 30° and 60° respectively. Far fewer active nuclei would be expected at these temperatures, and dendritic growth rates from the nucleation sites would also be considerably slowed. A better comparison of the effect of velocity would likely have been obtained by keeping a constant total temperature rather than static temperature, as in these tests.

Premature nucleation may occur on some occasions, particularly at higher speeds, because of the presence in the air stream of a few ice (frost) crystals blown off the heat exchanger tubes in the wind tunnel. Such ice crystals are not considered sufficient to effect normal icing characteristics.

They may however be responsible for the difference in nucleation delay between Tests 21 and 44 (Table IV), although another factor is that dry air surface temperatures were some 1°C cooler in Test 44 than in Test 21.

Figures 21 and 22, besides showing the nucleation delays in Tests 36 and 31 respectively, also show the elimination of any delay when ice crystals were present in significant numbers, as in the corresponding mixed condition Tests 37 and 32.

The ripples seen during the temperature rise portion of Figs. 21(a), 22(b) and 23(b) are artifacts of the simulation method, in Fig. 21(a) caused by instability of the water spray nozzles at the very low water flow rate necessary at the low speed, low L.W.C. condition, while in Figs. 22(b) and 23(b) caused by instability in the operation of the snow crystal nozzle. The ripples seen in Fig. 24 may be caused by spray nozzle instability, but this is not considered likely at the water flow rate used in Test 21. A more probable cause in this case is small nucleated ice crystals in the water film, not adhered to the cylinder and flowing over the thermocouples with the water film.

It is noticeable in Table IV that the delay is generally least at the stagnation point and increases with angle around the cylinder. If this was in fact the case, it is not easy to explain, as one would expect that water flowing away from the stagnation region would nucleate more readily than the fresh supply of water impinging there. However, perusal of Figs. 21(a), 22(a) and 24 suggests that, for at least angles up to 30°, if nucleation is taken to occur at the point where the temperature begins to rise from its minimum value, the nucleation delay time is about the same at each angle, about 4 seconds for Test 36, 0.8 seconds for Test 31 and about 8.5 seconds for Test 21. The longer nucleation delay observed at 60° may in fact be more apparent than real and may in part be due to the lower droplet impingement rate at this angle together with the streaming of runback water, resulting in incomplete or intermittent wetting of the thermocouple junction.

Figure 23 compares corresponding liquid only and mixed condition tests at -15°C but at high velocity, 122 m/s. No nucleation delay is evident here, nor in Fig. 25 which compares two liquid only cases at -15°C and 91.5 m/s with liquid water contents of 0.4 g/m^3 and 1.2 g/m^3.

Evident in Figs. 21, 22, 23 and 25 is the contribution of the thermal capacity and thermal conductivity of the cylinder and/or thermocouples to the heat balance during the initial transient response to the icing process. As proportionately more heat is adsorbed by the cylinder relative to the resultant of the other heat sources and sinks, the time constant of the temperature response increases. This is seen by comparing Fig. 21(a) with Fig. 22(a), and Fig. 25(a) with Fig. 25(b), where the change in both cases is caused by a change in liquid water content. Correspondingly, a change in velocity is seen to have a similar effect, c.f. Fig. 25(a) and Fig. 23(a).

From these recordings, the maximum temperature achieved at each thermocouple location was measured for all tests. As long as this maximum temperature occurred sufficiently early in the run, i.e. before a significant

ice thickness had built up which could have insulated the thermocouple junctions, then this measured temperature should have approximated closely to the icing surface temperature. In actual fact the maximum temperature occurred for all tests within 30 seconds from the start of the test, and in most cases sooner than 20 seconds. It is worthy of note that for all tests resulting in rates of ice accretion greater than 1.0 mm^2/s, the maximum temperature was recorded within 2 to 3 seconds from the start of icing, see for instance Test 42 (Fig. 25(b)) where the maximum occurred at a little over one second, the temperature thereafter decreasing as the insulating effect of the ice became felt.

These maximum (ice surface) temperatures are tabulated in Tables V and VI for liquid only and mixed conditions respectively. Temperature errors of up to about $\pm 0.3°C$ are apparent from these results, possibly as a result of galvanometer zero errors, thermocouple calibration errors, trace reading errors (as a result of a broad trace or noise on the trace), the insulating effect of ice, conduction into the substrate, or a combination of some or all of these.

The results for liquid water only at a nominal temperature of -15°C and L.W.C. of 0.4 g/m^3 are presented in Fig. 26, together with computed results using the mathematical model of Ref. 1. The results for -15°C with L.W.C. of 1.2 g/m^3 are shown in Fig. 27, while Fig. 28 presents all liquid water only test results at a nominal -5°C.

In these three figures, the solid lines are the model results computed at the nominal temperature and liquid water content, using either the smooth or rough cylinder heat transfer coefficient formulation (see Ref. 1) as indicated. Where broken lines are shown, these are the model results using the actual air temperature and liquid water content for the particular test.

Test 14 (Figs. 5, 6 and 26(a)) is clearly, both in appearance and shape and in its surface temperature profile, entirely within the dry ice growth (rime) regime. It seems reasonable to use the smooth heat transfer coefficient in this case (except perhaps in the feathery region beyond 60°), and in fact when actual parameter values are employed in the model, extraordinary good agreement between experimental and model-predicted temperatures are achieved. If this agreement is real and not fortuitous, it suggests that wind tunnel turbulence effects are not significant.

Tests 41 (Figs. 3,5,6 and 26(b)) and 40 (Figs. 7,8 and 27(a)) are by appearance and shape of intermediate form wherein the stagnation region is of marginally wet growth, and the question arises as to whether a smooth or a rough heat transfer coefficient should be employed in the model. Figs. 26(b) and 27(a) both suggest that the smooth cylinder coefficient slightly underestimates the convective and evaporative losses, while the rough cylinder formulation assumed rather seriously overestimates these losses.

All other liquid only tests at -15°C are clearly in the wet growth (mushroom) regime, and it appears from Figs. 27(b),(c) and (d) that as the wetness increases the effective heat transfer coefficient increases from something less than the rough cylinder value used to greater than that used in the model

predictions. On the other hand, on an icing growth rate basis, Fig. 13 suggests that in the wet growth regime the stagnation point heat transfer coefficient should be greater than that assumed in the model if better agreement with observed growth rates is to be achieved. Another reason for this latter discrepancy that was put forward in Ref. 1 was the possible existence of "spongy" ice, and the cracks which occurred in the ice deposit at the end of several tests at the two higher speeds (Figs. 6 and 8) might perhaps be taken as evidence of this. However, it is believed that these cracks are more probably the result of the slight drag induced deflection of the cylinder being relieved by the reduction of air speed at completion of the run, together with the cooling and consequent contraction and embrittlement of the ice on cessation of the icing sprays.

Similar comparisons between experimental temperature measurements and those predicted by the model for the liquid only tests at -5°C nominal temperature are shown in Fig. 28. All of these tests are in the wet growth regime, and the rough cylinder heat transfer coefficient has been assumed in the model predictions.

It should be remembered that all these temperature measurements were within 30 seconds of the start of each test (in fact, within 3 seconds for Test 25, Fig. 26(c) and for Tests 16,42 and 45, Fig. 27) so that the ice accretions had not developed to the extents shown in Figs. 5 through 12. The profiles would still be essentially cylindrical, although the nature and degree of roughness would not necessarily be uniform around the cylinder.

The temperature profiles for the various mixed condition tests are shown in Figs. 29, 30, 31 and 32. In Fig. 29 the results for the three tests at nominal conditions of -15°C and 0.4 g/m^3 L.W.C. are shown; the smooth cylindrical profile that was assumed in the model results in over-prediction of the temperatures, not because this assumption was necessarily wrong, but because the physical processes assumed in the mixed icing model were incorrect. When the model was run using an equivalent liquid water content (broken lines in Fig. 29) based on rotating cylinder measurements (Section 4.2 and Table III) good agreement, perhaps fortuitously, was achieved between actual and model temperatures, particularly at a velocity of 61 m/s (Fig. 29(b)).

Agreement is again achieved between measured and model temperatures at 61 m/s with -15°C air temperature and 1.2 g/m^3 L.W.C. (Test 17, Fig. 30(a)) when an equivalent L.W.C. based on Table III is used. However, at 122 m/s (Test 47, Fig. 30(b)) the measured temperatures seem to agree with the mixed condition model-prediction, presumably coincidentally because of the false assumptions in the model.

Figures 31 and 32 show the results of mixed condition tests at a nominal air temperature of -5°C. Most of these tests were observably in the wet growth regime (Figs. 9 and 11) and this is confirmed by the temperature measurements which with a few exceptions indicated 0°C (within the general accuracy of the measurements). Of the exceptions, Test 37 is clearly dry growth as both the photograph (Fig. 9) and the temperature measurements (Fig. 31(a)) indicate. One might suspect from the profile shapes that Test 20 (Fig. 10) and Test 32 (Fig. 12)

are both in the dry growth regime; however, the photographs (Figs. 9 and 11) suggest and the temperature measurements (Figs. 31(c) and 32(a)) confirm that wet growth actually prevailed.

Fig. 31(c) shows that in Test 39 the frontal part of the cylinder to an angle of at least ±30° was at a temperature above 0°C in conformity with the fact that no ice formed on the cylinder at angles up to about ±70°C.

5.0 CONCLUSIONS

1. The most significant conclusion from these experiments is that the size of ice particles used in mixed condition icing tests has a significant effect on the characteristics of the resulting ice accretion. Small ice particles, such as produced by a "snow" nozzle, act as efficient freezing nuclei for the supercooled water droplets that provide the liquid phase of the mixed condition, resulting in an unknown mix of liquid water and ice at the wind tunnel test section. It is clear that if such a condition could occur in nature, it would be a highly transient event and the likelihood of experiencing the type of ice accretions observed in these tests would be negligible. One must therefore question the validity of using snow nozzles for the simulation of mixed phase clouds unless the particle size can be made significantly larger than that of the supercooled water droplets, while at the same time ensuring complete freezing of the particles.

2. The cylinder surface temperature measurements threw considerable light on the nature of the icing process, and in particular confirmed the validity of the mathematical model developed in Ref. 1 in the dry growth regime of ice accretion in liquid phase clouds.

3. In the wet growth regime, it has been seen that the heat transfer coefficient around the cylinder varies with the degree of wetness, even before sufficient ice has been formed to significantly modify the basic cylindrical shape. Considerable work appears necessary in this area.

4. The temperature measurements have helped to confirm the existence of the nucleation delay which had previously only been observed in a very qualitative sort of way. This delay appeared to be greater the lower the water impingement rate and the higher the total temperature. Such delays are probably not very significant in the final outcome of an icing encounter, and in any event it should be remembered that distilled water is used in the wind tunnel; the comparative nucleating characteristics of natural atmospheric water are not known.

6.0 REFERENCES

1. Lozowski, E. P.
Stallabrass, J. R.
Hearty, P. F.
The Icing of an Unheated Non-Rotating Cylinder in Liquid Water Droplet-Ice Crystal Clouds. National Research Council, Report LTR-LT-96, 1979.

2. Miner, D. F.
Seastone, J. B.
Handbook of Engineering Materials. Wiley Engineering Handbook Series, New York, 1955.

3. -- Wood Handbook. U. S. Department of Agriculture, Agriculture Handbook No. 72, 1955.

4. Stallabrass, J. R. An Appraisal of the Single Rotating Cylinder Method of Liquid Water Content Measurement. National Research Council, Report LTR-LT-92, 1978.

5. Langmuir, I.
Blodgett, K. B. A Mathematical Investigation of Water Drop Trajectories. AAF Tecnical Report No. 5418, 1946.

6. Dickey, T. A. An Analysis of the Effects of Certain Variables in Determining the Form of an Ice Accretion. U. S. Navy, Aeronautical Engine Laboratory Report No. AEL-1206, 1952.

3. -- Wood Handbook. U. S. Department of Agriculture, Agriculture Handbook No. 72, 1955.

4. Stallabrass, J. R. An Appraisal of the Single Rotating Cylinder Method of Liquid Water Content Measurement. National Research Council, Report LTR-LT-92, 1978.

5. Langmuir, I.
Blodgett, K. B. A Mathematical Investigation of Water Drop Trajectories. AAF Tecnical Report No. 5418, 1946.

6. Dickey, T. A. An Analysis of the Effects of Certain Variables in Determining the Form of an Ice Accretion. U. S. Navy, Aeronautical Engine Laboratory Report No. AEL-1206, 1952.

TABLE I

SUMMARY OF TEST CONDITIONS AND ICING RESULTS
AT A NOMINAL AIR TEMPERATURE OF -15°C

Test No.	Air Speed m/s	Actual[1] Air Temp. °C	L.W.C. g/m^3	I.C.C. g/m^3	Icing Duration min.	Stagn Growth Rate μm/s	Ice Cross-Section mm^2	Ice Accretion Rate mm^2/s	Calcd[2] Accretion Rate mm^2/s
24	30.5	-14.1	0.40	1.2	5.00	9.5	44	0.15	0.18
40	30.5	-14.9	1.21	--	4.00	24.3	119	0.50	0.56
14	61	-15.6	0.39	--	2.50	22.0	72	0.48	0.44
15	61	-15.6	0.39	0.4	2.50	13.9	47	0.31	0.44
16	61	-15.4	1.24	--	2.50	49.1	224	1.49	1.40
17	61	-15.5	1.24	0.6	2.50	48.6	141	0.94	1.40
49	61	--	0.60	--	2.50	30.8	118	0.79	0.68
41	91.5	-15.4	0.40	--	2.50	31.3	112	0.75	0.73
42	91.5	-15.2	1.19	--	2.00	58.4	196	1.64	2.18
25	122	-15.6	0.43	--	2.50	38.1	177	1.18	1.10
26	122	-15.2	0.43	0.95	2.68	30.6	86	0.54	1.10
45	122	-15.6	1.20	--	1.00	63.5	125	2.08	3.07
47	122	-16.0	1.18	0.95	1.00	76.6	138	2.31	3.02

Notes:

(1) Actual Air Temperatures were deduced from the cylinder surface temperatures in dry air immediately preceding the start of icing. Where no actual temperature is shown, a dry air measurement was not made.

(2) These Accretion Rates calculated for the liquid component only using Langmuir and Blodgett[5] total collection efficiency data for droplets of 20 μm diameter, and assuming an ice density of 890 kg/m^3, and that all impinging water is retained as ice.

TABLE II

SUMMARY OF TEST CONDITIONS AND ICING RESULTS
AT A NOMINAL AIR TEMPERATURE OF -5°C

Test No.	Air Speed m/s	Actual[1] Air Temp. °C	L.W.C. g/m^3	I.C.C. g/m^3	Icing Duration min.	Stagn Growth Rate μm/s	Ice Cross-Section mm^2	Ice Accretion Rate mm^2/s	Calcd[2] Accretion Rate mm^2/s
36	30.5	-5.2	0.40	--	5.00	7.6	62	0.21	0.18
37	30.5	-5.1	0.40	1.0	5.00	20.9	53	0.18	0.18
31	30.5	-4.3	1.18	--	5.00	14.9	160	0.53	0.54
32	30.5	-4.4	1.18	1.2	5.00	39.5	156	0.52	0.54
18	61	-4.5	0.39	--	4.00	13.8	122	0.51	0.44
19	61	-5.2	0.39	0.3	4.00	19.7	87	0.36	0.44
20	61	-4.8	0.39	0.6	4.00	25.2	75	0.31	0.44
46	61	-5.8	1.20	--	2.52	18.2	155	1.02	1.36
48	61	-5.8	1.17	0.6	2.50	51.3	195	1.30	1.32
21	91.5	-4.6	0.40	--	4.00	8.1	60	0.25	0.73
38	91.5	--	0.40	1.0	2.50	42.8	164	1.09	0.73
44	91.5	-5.8	1.19	--	1.50	11.3	84	0.94	2.18
39	122	-6.3	0.38	0.95	2.50	0	50	0.33	0.97

Notes:

(1) Actual Air Temperatures were deduced from the cylinder surface temperature in dry air immediately preceding the start of icing. Where no actual temperature is shown, a dry air measurement was not made.

(2) These Accretion Rates calculated for the liquid component only using Langmuir and Blodgett[5] total collection efficiency data for droplets of 20 μm diameter, and assuming an ice density of 890 kg/m^3, and that all impinging water is retained as ice.

TABLE III

EFFECT OF ICE PARTICLES ON THE EQUIVALENT LIQUID WATER CONTENT DERIVED BY THE ROTATING CYLINDER METHOD

Air Speed m/s	Static Air Temp. °C	L.W.C. g/m^3	Ice Crystal Content g/m^3	Snow Nozzle Air Press. kPa(ga)	Equiv.* L.W.C. g/m^3	Ratio: Equiv. L.W.C. / True L.W.C.
30.5	-13	0.40	1.0	480	0.22	0.55
61	-15	0.42	0.4	345	0.24	0.57
91.5	-15	0.40	1.0	480	0.19	0.48
122	-15	0.38	0.95	480	0.21	0.55
61	-15	1.15	0	--	1.15	1.0
61	-15	1.15	0.6	345	0.62	0.54
61	-15	1.15	0.6	480	0.57	0.50
61	-5	0.42	0	--	0.40	0.95
61	-5	0.42	0.3	345	0.32	0.76
61	-5	0.42	0.6	345	0.33	0.79
61	-5	0.42	0.6	480	0.30	0.71

* The Equivalent Liquid Water Content is the L.W.C. given by the Rotating Cylinder Method assuming that the accreted mass of ice was the result of supercooled liquid water droplets only.

TABLE IV

NUCLEATION DELAY TIMES FOR LIQUID ONLY TESTS

Test No.	Air Speed m/s	Air Temp. °C	L.W.C. g/m^3	Nucleation Delay, s			
				$\alpha = -15°$	$\alpha = 0°$	$\alpha = 30°$	$\alpha = 60°$
40	30.5	-14.9	1.21	0.3	0.8	1.2	1.5
14	61	-15.6	0.39	0.1	0	0.1	0
16	61	-15.4	1.24	0.1	0.1	0.1	0.1
41	91.5	-15.4	0.40	0	0	0	0.1
42	91.5	-15.2	1.19	0	0	0	0.1
25	122	-15.6	0.43	0	0	0	0.15
45	122	-15.6	1.20	0	0	0	0
36	30.5	-5.2	0.40	4.7	4.4	5.5	8.0
31	30.5	-4.3	1.18	1.5	0.85	1.4	2.5
18	61	-4.5	0.39	0.8	0.6	1.0	2.5
46	61	-5.8	1.20	0.1	0.25	0.5	0.8
21	91.5	-4.6	0.40	11.2	11.0	11.3	18.0
44	91.5	-5.8	1.19	0.1	0	0.1	0.4

TABLE V

MEASURED ICING TEMPERATURES AROUND CYLINDER
FOR TESTS WITH LIQUID WATER ONLY

Test No.	Air Speed m/s	Air Temp. °C	L.W.C. g/m^3	Icing Temperature - °C			
				$\alpha = 0°$	$\alpha = 15°$	$\alpha = 30°$	$\alpha = 60°$
14	61	-15.6	0.39	-4.3	-4.6	-5.9	-10.6
41	91.5	-15.4	0.40	-0.9	-0.9	-3.0	-9.1
25	122	-15.6	0.43	-0.3	-0.25	-0.6	-8.1
40	30.5	-14.9	1.21	-0.5	-0.5	-1.8	-8.4
16	61	-15.4	1.24	-0.3	-0.3	-0.35	-6.4
42	91.5	-15.2	1.19	-0.3	-0.1	-0.6	-6.8
45	122	-15.6	1.20	+0.3	+0.1	-0.3	-5.6
36	30.5	-5.2	0.40	-0.35	-0.4	-1.2	-4.0
18	61	-4.5	0.39	+0.3	+0.25	+0.1	-1.4
21	91.5	-4.6	0.40	+0.3	+0.25	+0.1	-0.6
31	30.5	-4.3	1.18	-0	-0	+0.1	-0.2
46	61	-5.8	1.20	-0	+0.1	-0.1	-0.4
44	91.5	-5.8	1.19	-0.2	-0	+0.2	-0.2

TABLE VI

MEASURED ICING TEMPERATURES AROUND CYLINDER
FOR TESTS IN MIXED CONDITIONS

Test No.	Air Speed m/s	Air Temp. °C	L.W.C. g/m^3	I.C.C. g/m^3	Icing Temperature - °C			
					$\alpha = 0°$	$\alpha = 15°$	$\alpha = 30°$	$\alpha = 60°$
24	30.5	-14.1	0.40	1.2	-8.5	-8.7	-9.0	-11.3
15	61	-15.6	0.39	0.4	-7.8	-8.1	-8.8	-11.9
26	122	-15.2	0.43	0.95	-1.0	-0.7	-3.0	-8.0
17	61	-15.5	1.24	0.6	-0.35	-0.4	-1.5	-8.6
47	122	-16.0	1.18	0.95	-0.3		-0.5	-3.7
37	30.5	-5.1	0.40	1.0	-2.5	-1.7	-1.8	-3.1
19	61	-5.2	0.39	0.3	+0.1	+0.3	0	-1.9
20	61	-4.8	0.39	0.6	+0.3	+0.3	+0.1	-1.4 to -0.3
38	91.5	--	0.40	1.0	-0	-0	-0.1	-0.5
39	122	-6.3	0.38	0.95	+0.9	+0.6	+0.4	-0.2
32	30.5	-4.4	1.18	1.2	-0	-0	+0.2	-0.7
48	61	-5.8	1.17	0.6	-0		-0.4	-1.1

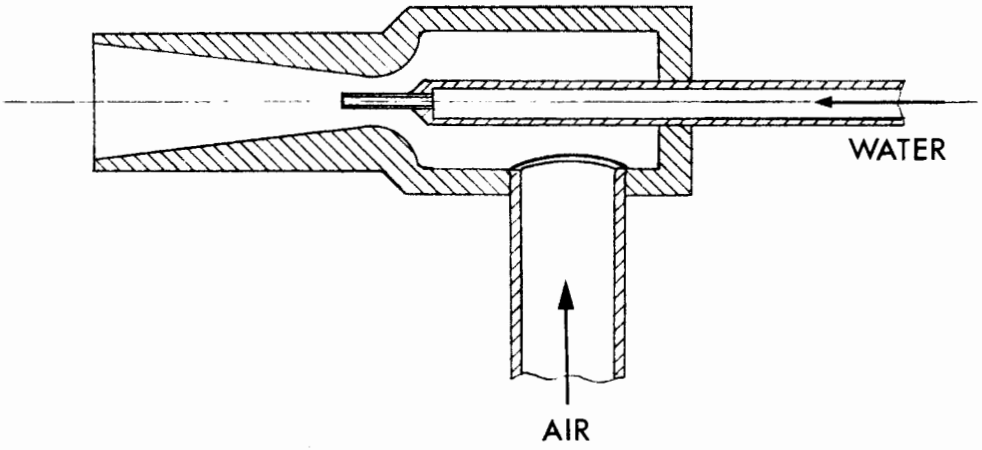

FIG. 1 MK II SNOW NOZZLE
(Full Size)

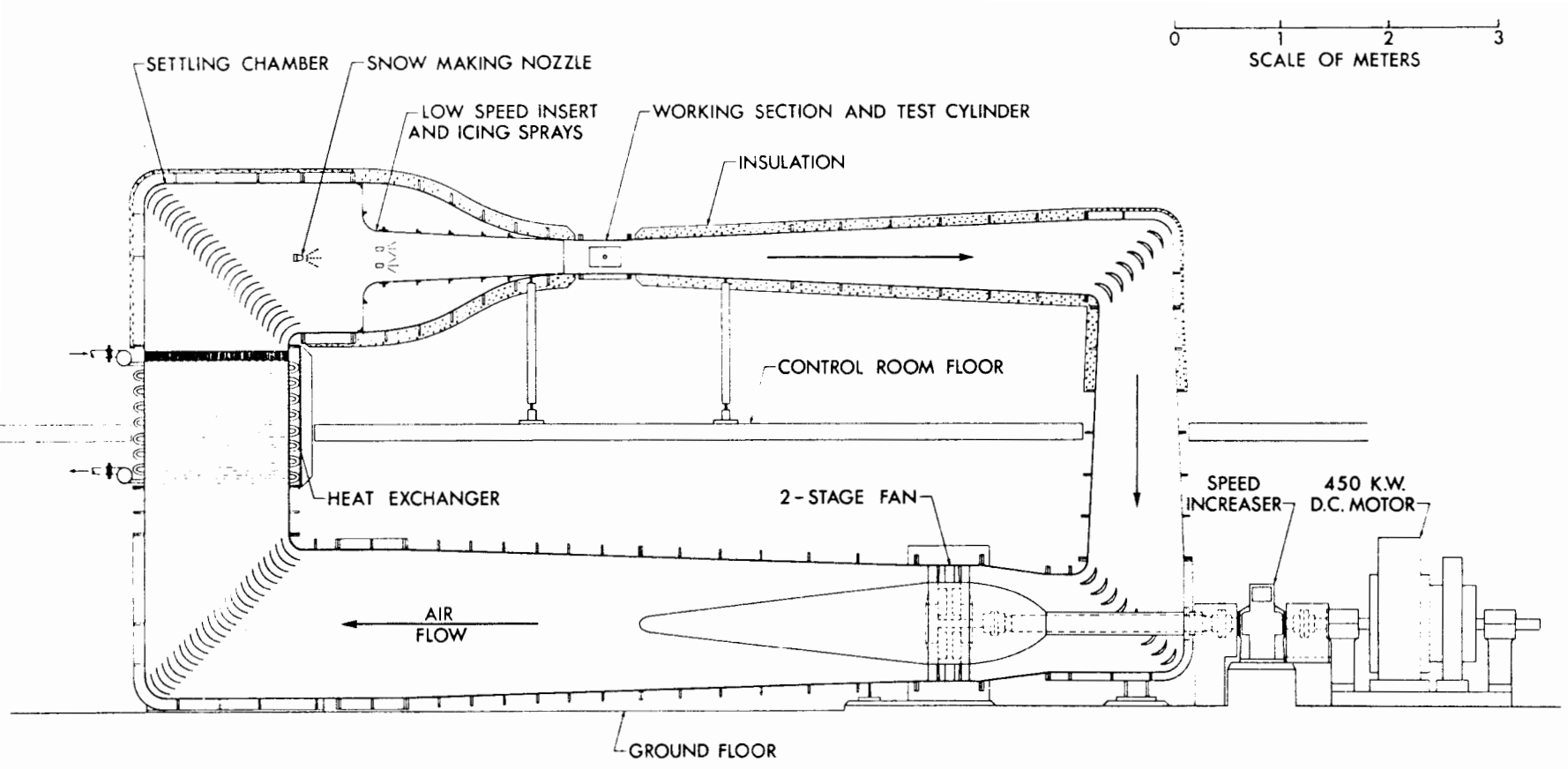

FIG. 2 HIGH SPEED ICING WIND TUNNEL

LTR-LT-105
Fig. 2

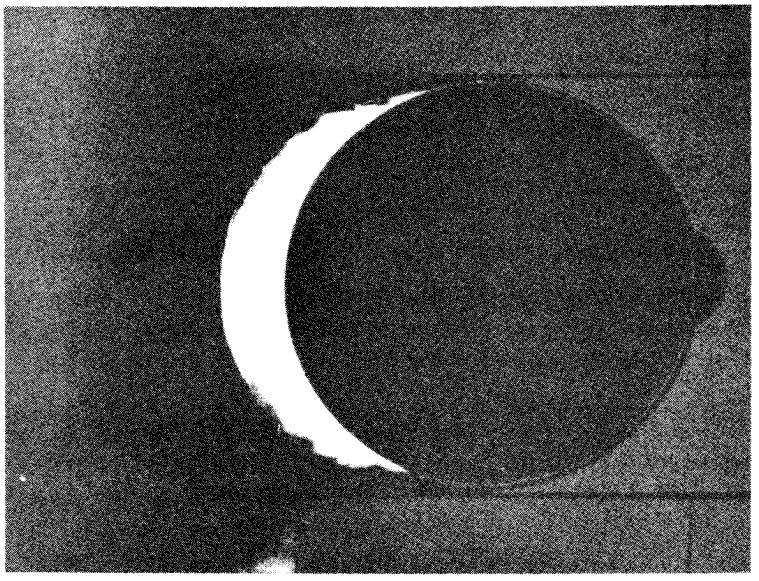

(a) Ice Profile by Plasticene Mould Method

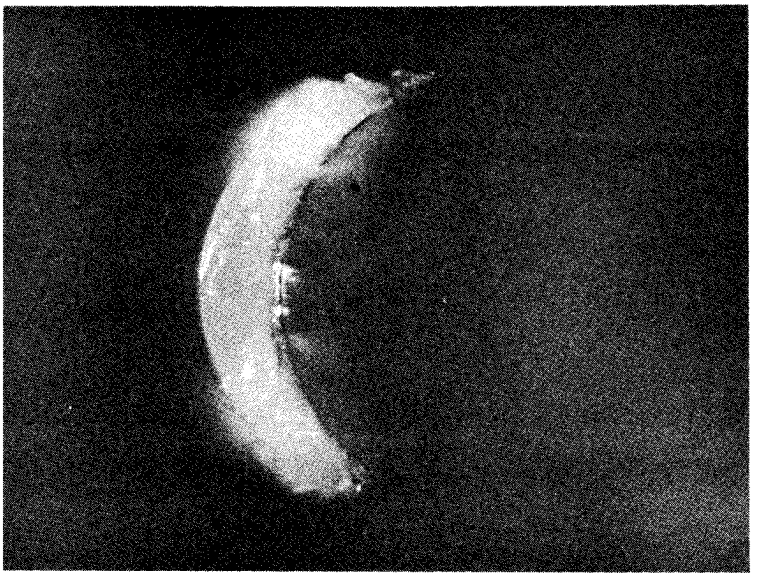

(b) Ice Profile by Ice Section Method

FIG. 3 METHODS OF RECORDING ICE PROFILE
(Test No. 41)

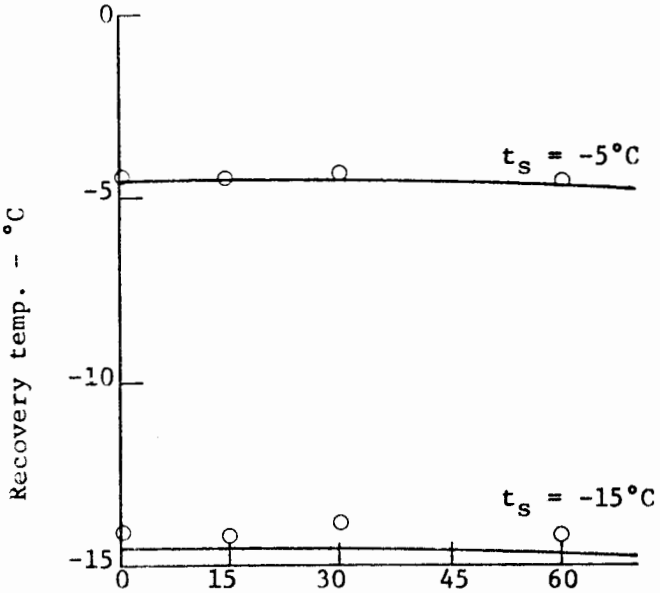

(a) V = 30.5 m/s

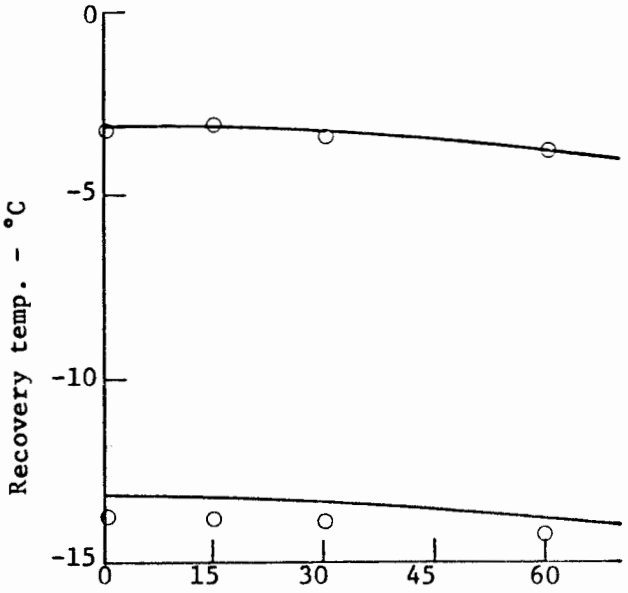

(b) V = 61 m/s

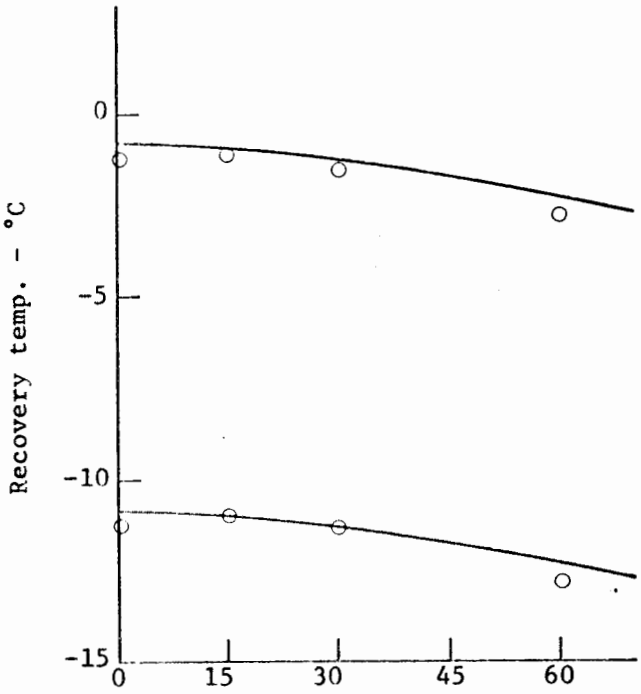

(c) V = 91.5 m/s

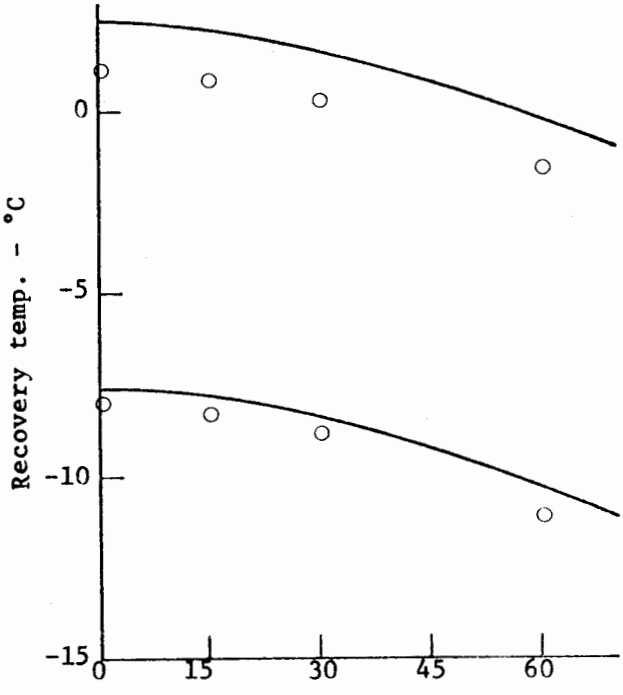

(d) V = 122 m/s

FIG. 4 DRY AIR RECOVERY TEMPERATURES FOR 0.0254 m DIAMETER CYLINDER

Points are average of measured values preceding all tests at noted velocity and nominal temperature. Lines are computed recovery temperatures using relation $r = 0.7 + 0.3 \cos 1.7\theta$

Air Speed - m/s

	30	61	92	122
Liquid only		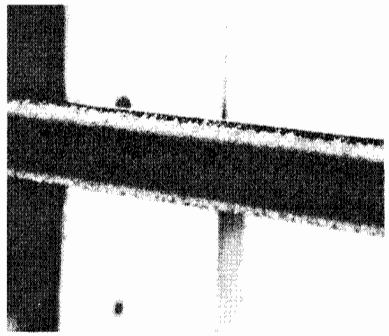	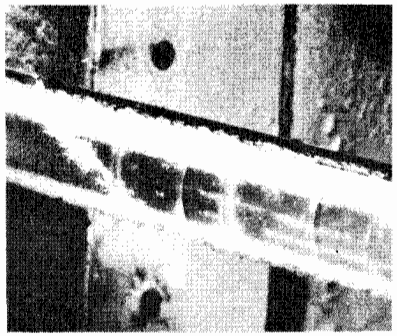	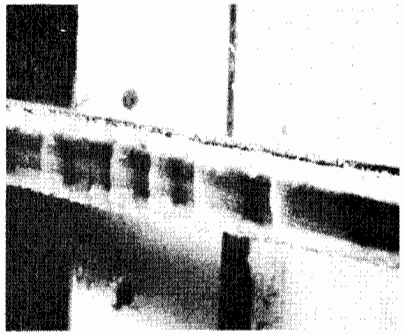
Liquid and Ice Crystals	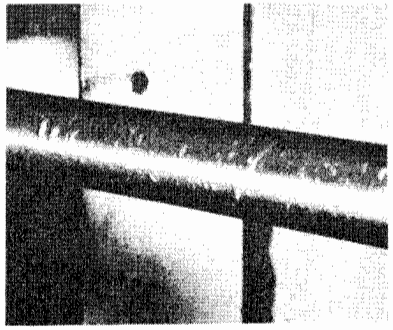	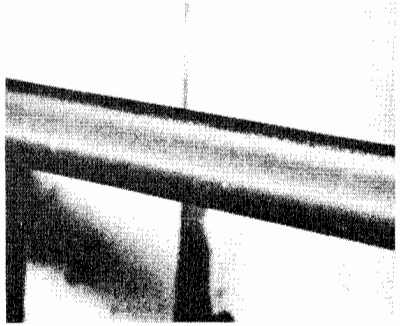		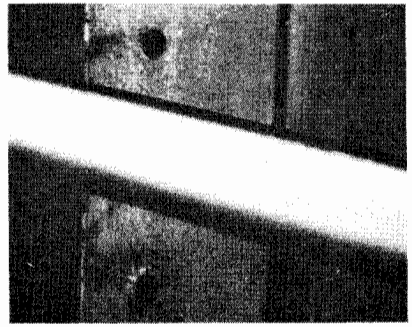
	I.C.C. = 1.2 g/m^3	I.C.C. = 0.4 g/m^3		I.C.C. = 0.95 g/m^3

FIG. 5 CYLINDER ICING AT -15°C AND L.W.C. = 0.4 g/m^3

COMPARISON BETWEEN LIQUID ONLY AND MIXED CONDITIONS

LTR-LT-105
Fig. 5

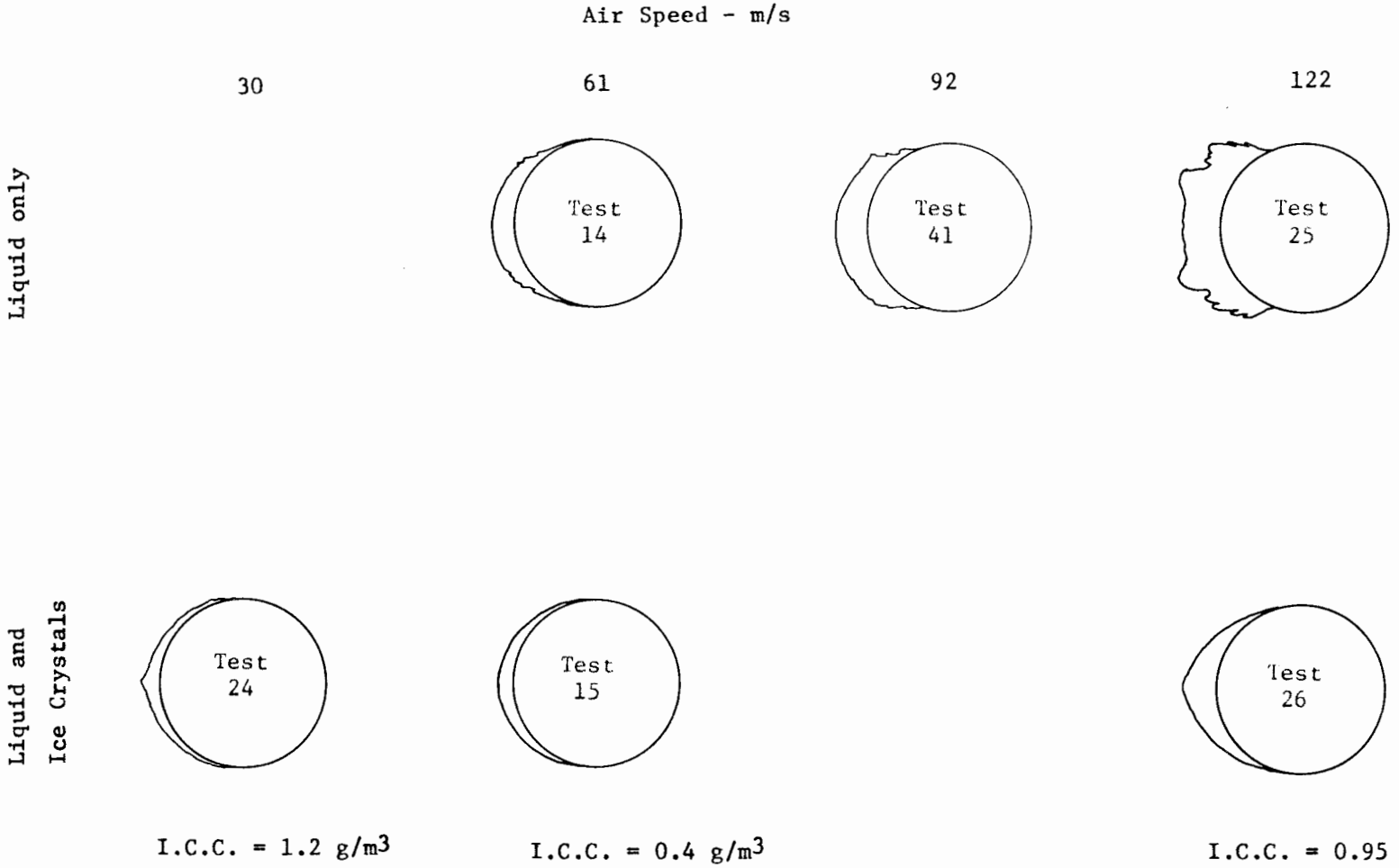

FIG. 6 CYLINDER ICING PROFILES AT -15°C AND L.W.C. = 0.4 g/m^3
COMPARISON BETWEEN LIQUID ONLY AND MIXED CONDITIONS

Air Speed - m/s

30 61 92 122

Liquid only

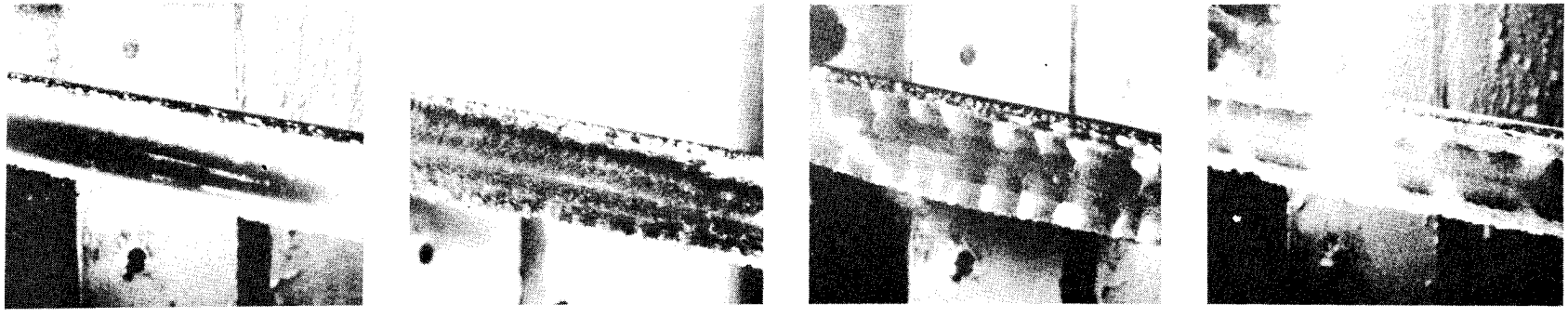

Liquid and Ice Crystals

I.C.C. = 0.6 g/m^3

I.C.C. = 0.95 g/m^3

FIG. 7 CYLINDER ICING AT -15°C AND L.W.C. = 1.2 g/m^3
COMPARISON BETWEEN LIQUID ONLY AND MIXED CONDITIONS

LTR-LT-105
Fig. 7

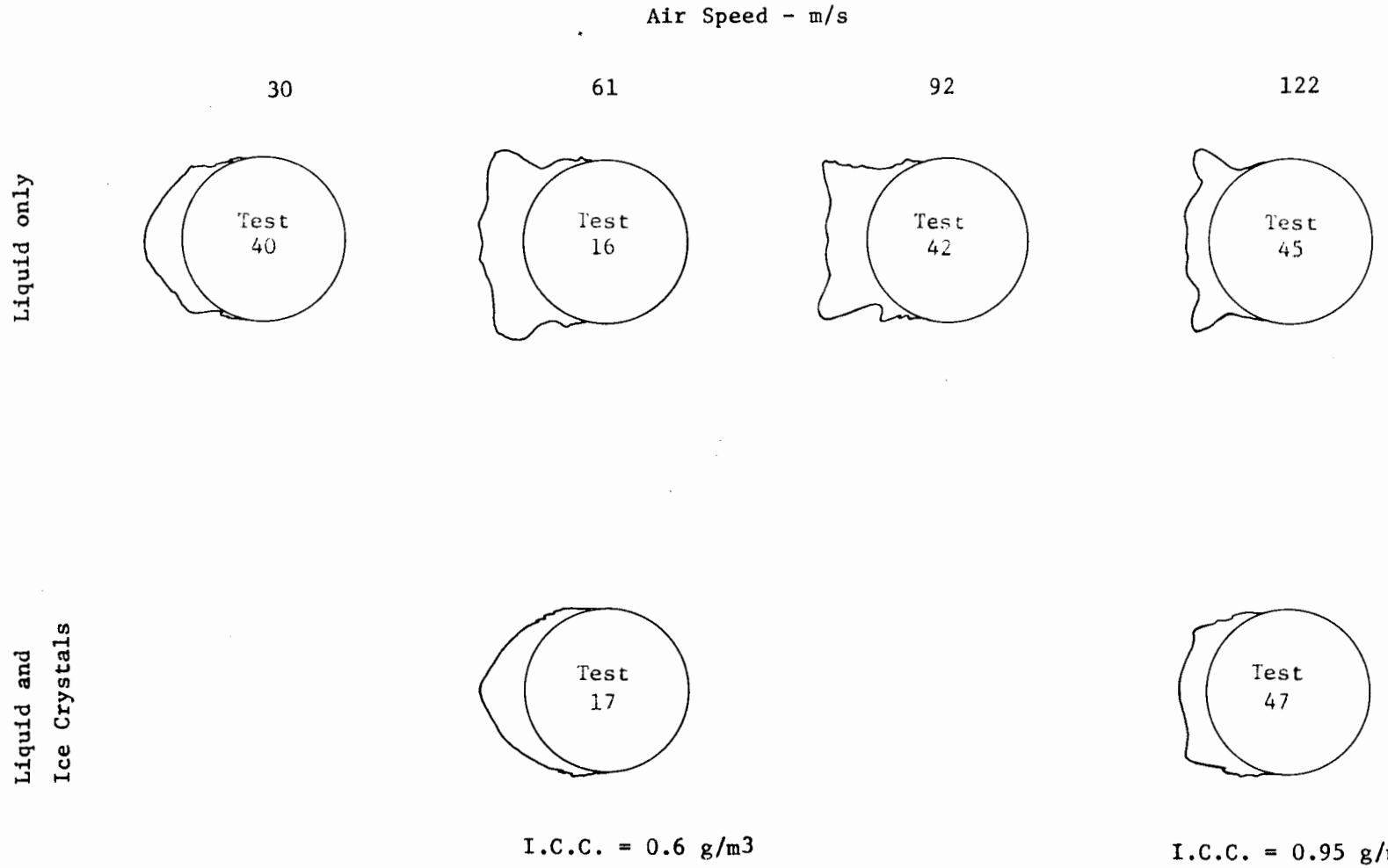

FIG. 8 CYLINDER ICING PROFILES AT -15°C AND L.W.C. = 1.2 g/m^3
COMPARISON BETWEEN LIQUID ONLY AND MIXED CONDITIONS

Air Speed - m/s

30 61 92 122

Liquid only

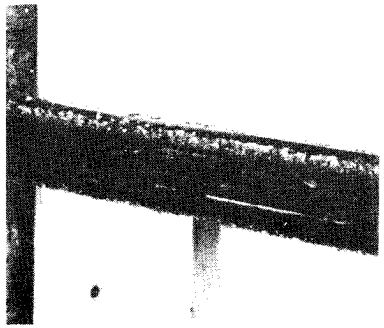

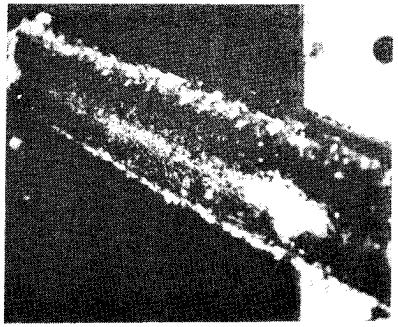

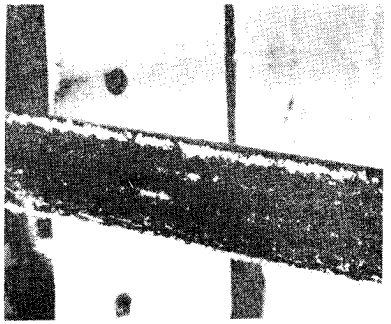

Liquid and Ice Crystals

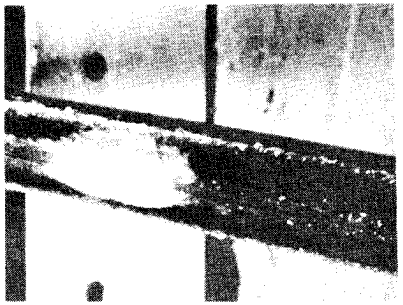

I.C.C. = 0.3 g/m^3

Liquid and Ice Crystals

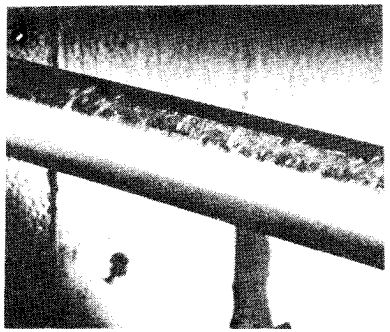

I.C.C. = 1.0 g/m^3

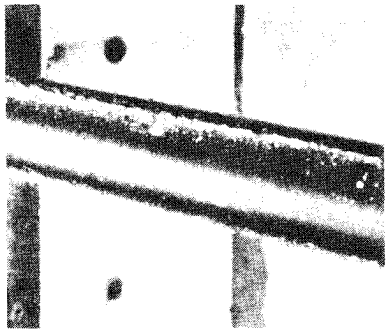

I.C.C. = 0.6 g/m^3

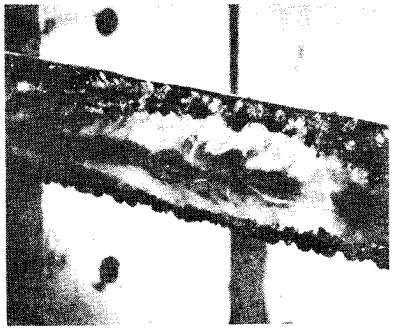

I.C.C. = 1.0 g/m^3

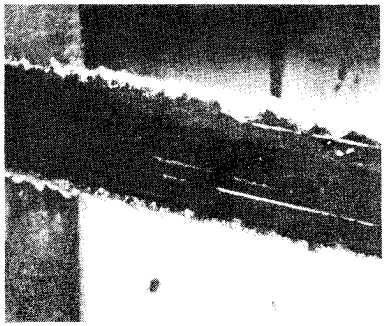

I.C.C. = 0.95 g/m^3

FIG. 9 CYLINDER ICING AT -5°C AND L.W.C. = 0.4 g/m^3
COMPARISON BETWEEN LIQUID ONLY AND MIXED CONDITIONS

LTR-LT-105
Fig. 9

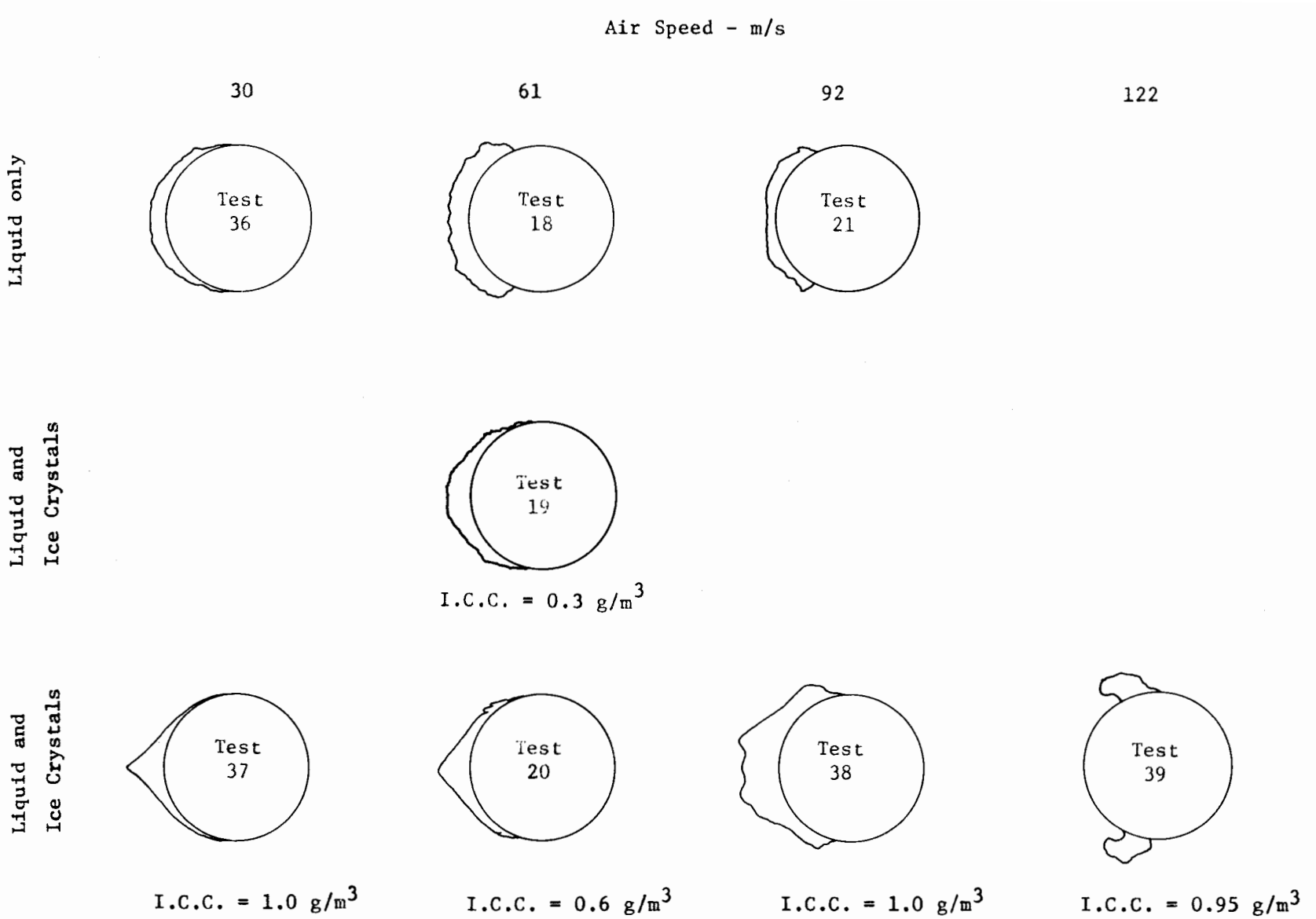

FIG. 10 CYLINDER ICING PROFILES AT -5°C AND L.W.C. = 0.4 g/m^3
COMPARISON BETWEEN LIQUID ONLY AND MIXED CONDITIONS

Air Speed - m/s

30 61 92 122

Liquid only

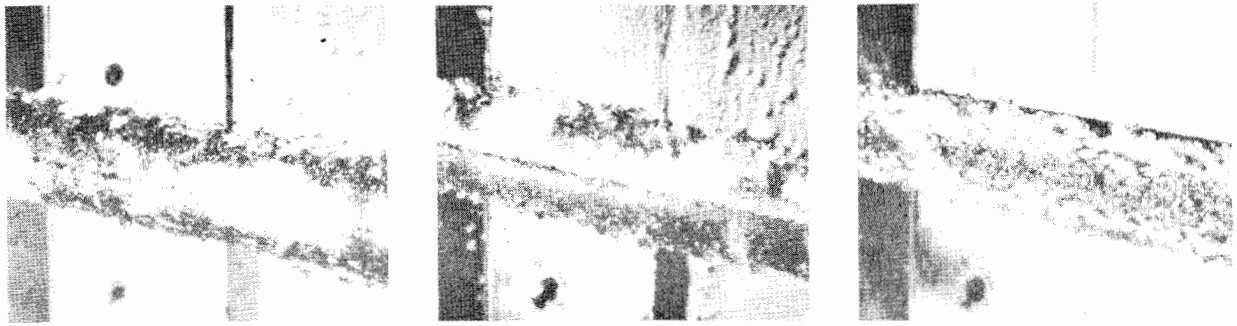

Liquid and Ice Crystals

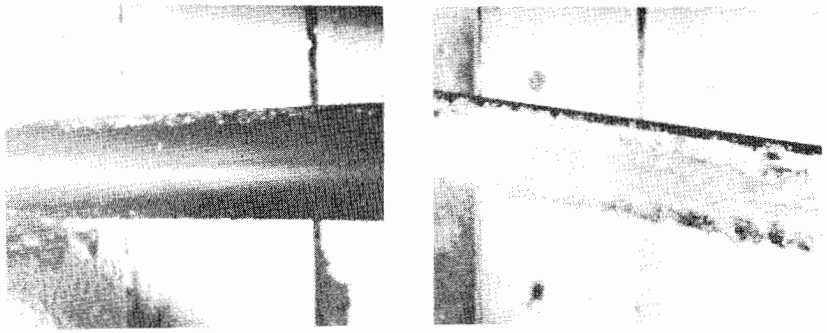

I.C.C. = 1.2 g/m^3 I.C.C. = 0.6 g/m^3

FIG. 11 CYLINDER ICING AT -5°C AND L.W.C. = 1.2 g/m^3
COMPARISON BETWEEN LIQUID ONLY AND MIXED CONDITIONS

LTR-LT-105
Fig. 11

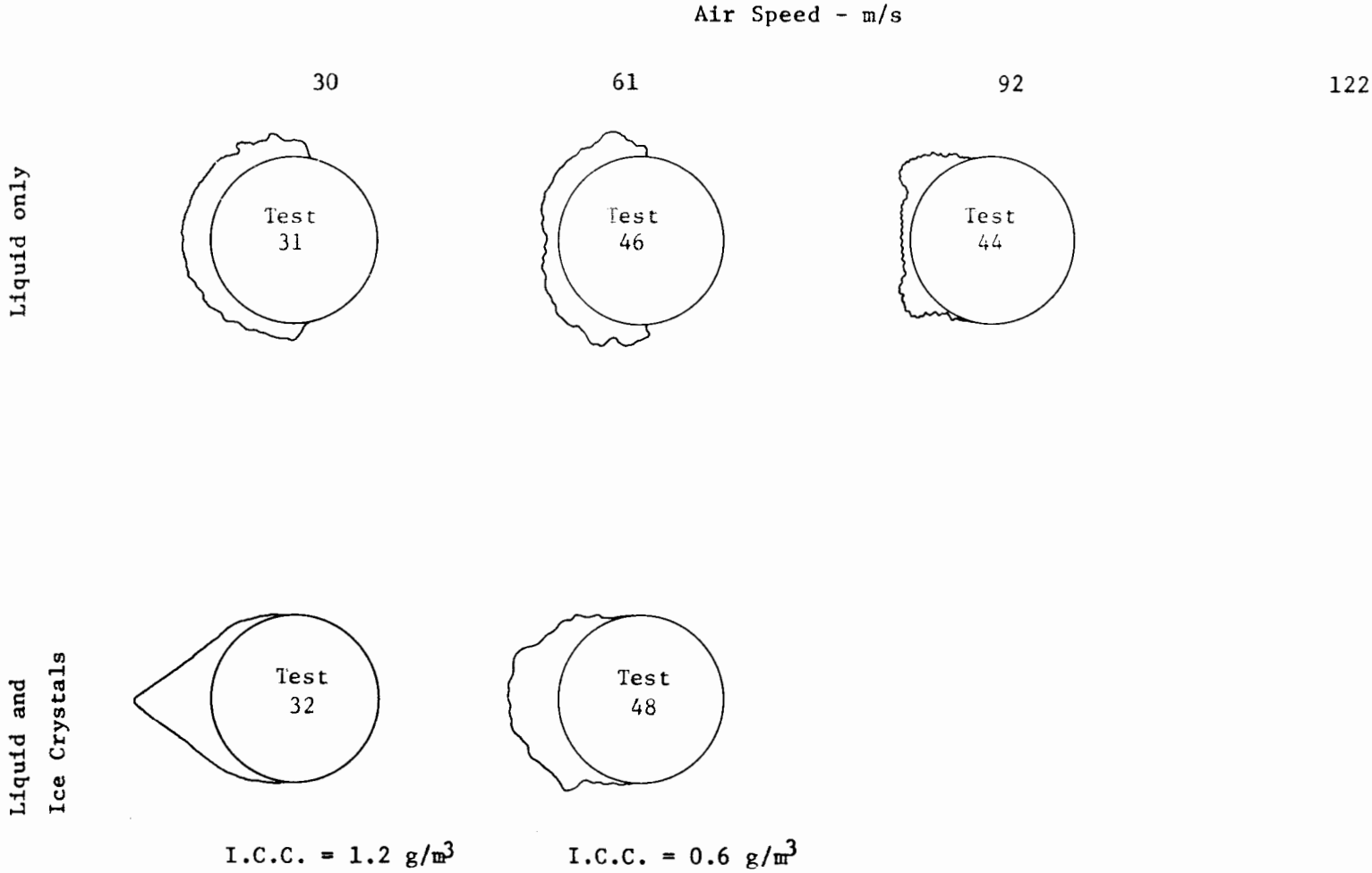

FIG. 12 CYLINDER ICING PROFILES AT -5°C AND L.W.C. = 1.2 g/m^3

COMPARISON BETWEEN LIQUID ONLY AND MIXED CONDITIONS

LTR-LT-105
Fig. 12

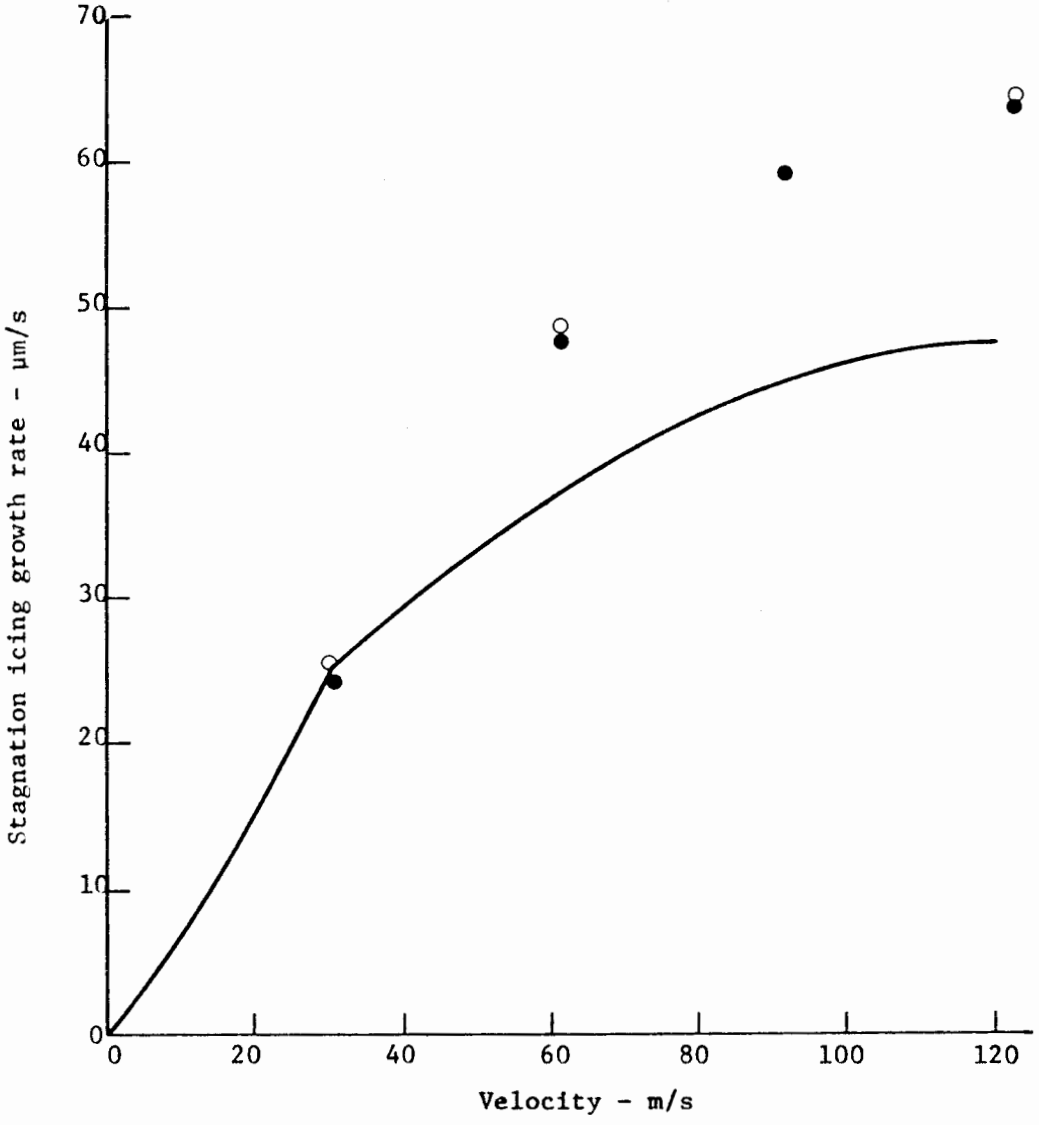

FIG. 13 STAGNATION LINE ICING RATE AT -15°C AND L.W.C. OF 1.2 g/m^3, LIQUID ONLY

Solid points are experimental values from these tests. Open points are from Ref. 1. Solid line is icing model prediction.

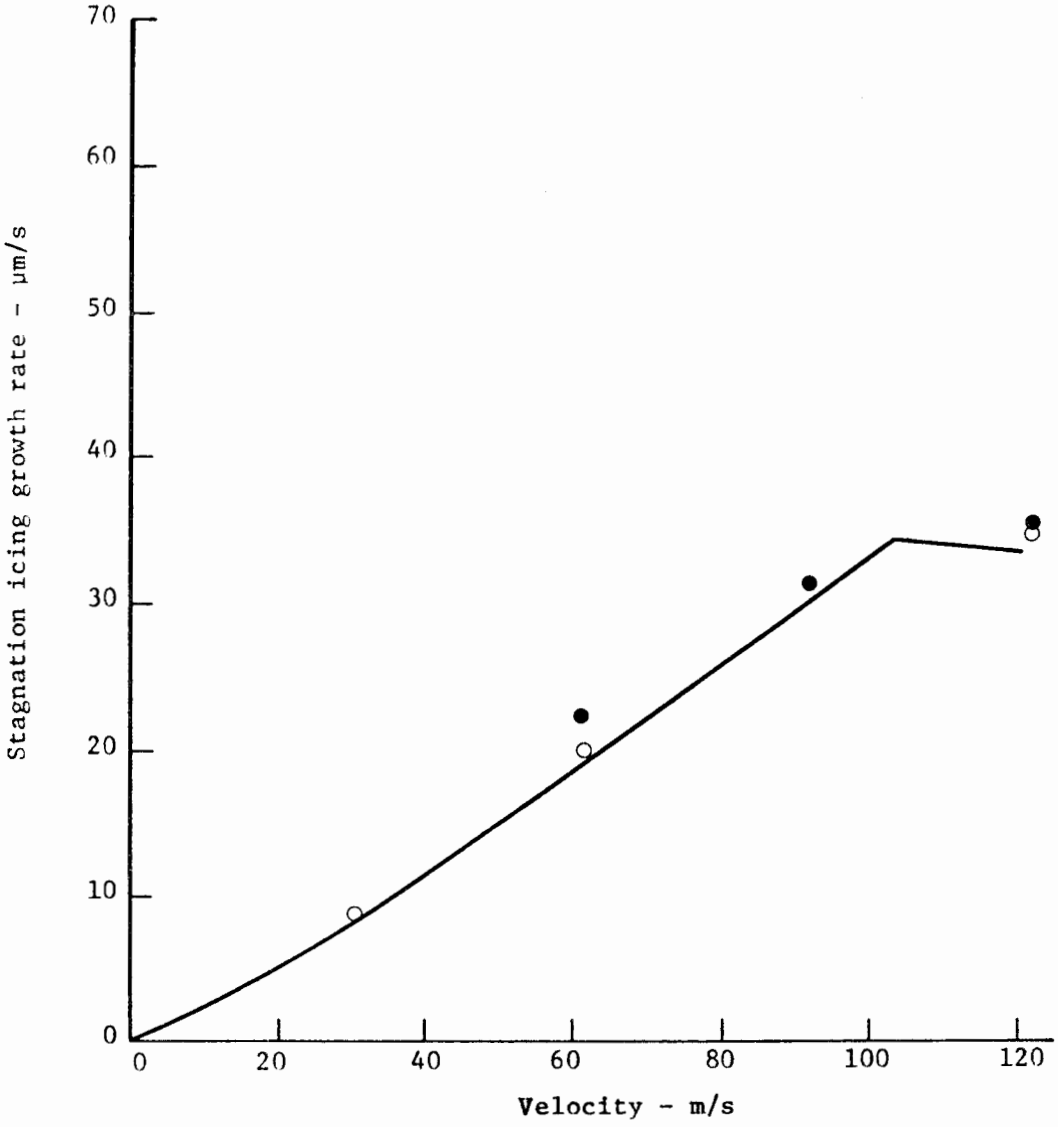

FIG. 14 STAGNATION LINE ICING RATE AT -15°C AND L.W.C. OF 0.4 g/m^3, LIQUID ONLY

Solid points are experimental values from these tests. Open points are from Ref. 1. Solid line is icing model prediction.

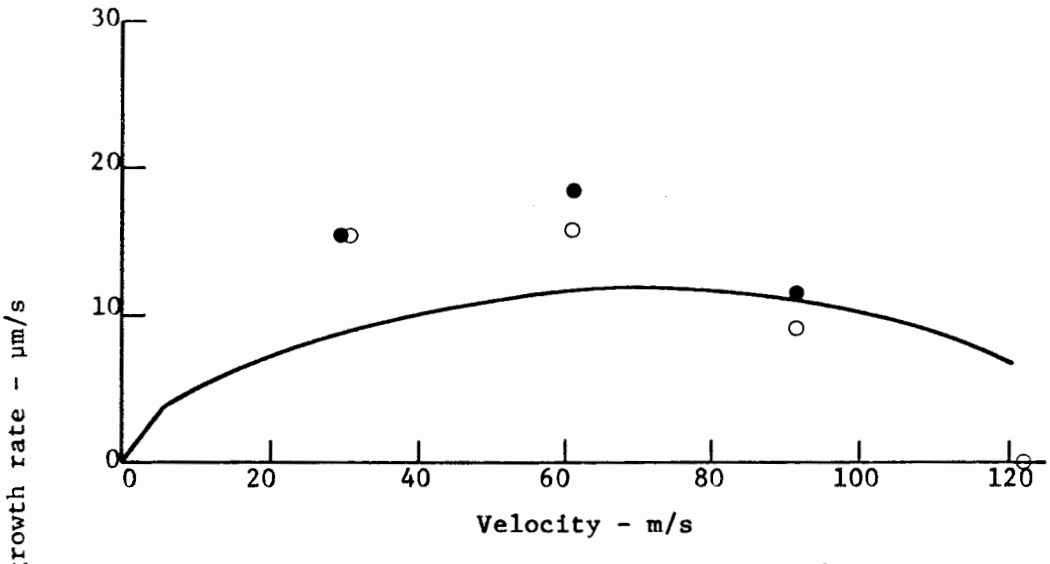

(a) Liquid water content = 1.2 g/m^3

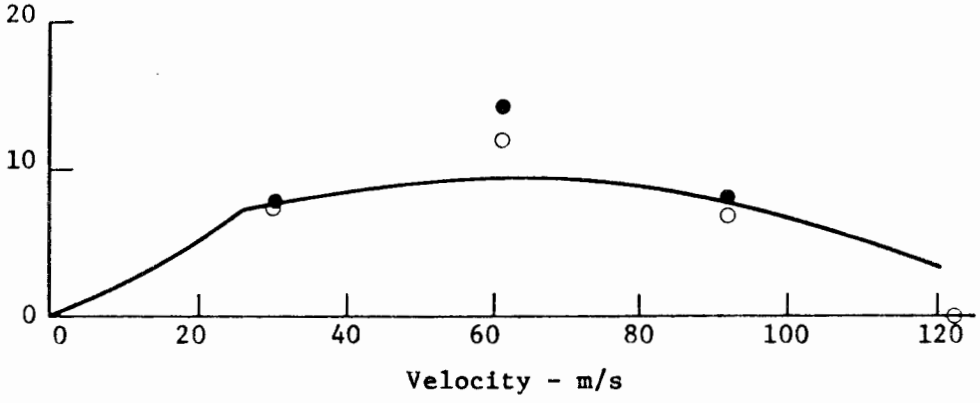

(b) Liquid water content = 0.4 g/m^3

FIG. 15 STAGNATION LINE ICING RATE AT -5°C, LIQUID ONLY

Solid points are experimental values from these tests. Open points are from Ref. 1. Solid line is icing model prediction.

From Ref. 1

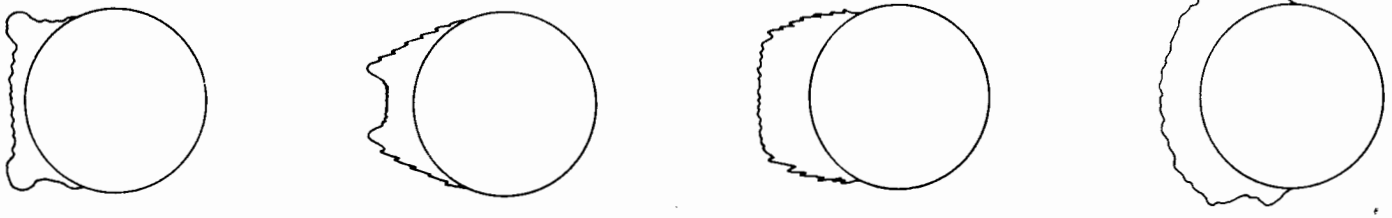

Present Tests

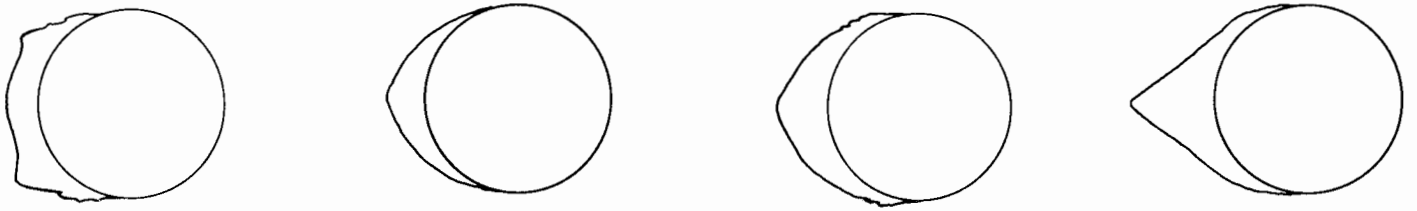

(a) T = -15°C
V = 122 m/s
L.W.C. = 1.2 g/m^3
I.C.C. = 1.0 g/m^3

(b) T = -15°C
V = 122 m/s
L.W.C. = 0.4 g/m^3
I.C.C. = 1.0 g/m^3

(c) T = -15°C
V = 61 m/s
L.W.C. = 1.2 g/m^3
I.C.C. = 0.6 g/m^3

(d) T = -5°C
V = 30 m/s
L.W.C. = 1.2 g/m^3
I.C.C. = 1.2 g/m^3

FIG. 16 COMPARISON OF ICE PROFILES OBTAINED IN PRESENT TESTS WITH THOSE OF REF. 1 FOR CORRESPONDING MIXED ICING CONDITIONS

Profiles of upper row from Ref. 1 using natural snow (d≈1 mm), those of lower row from present tests using ice crystal nozzle (d≈20 μm)

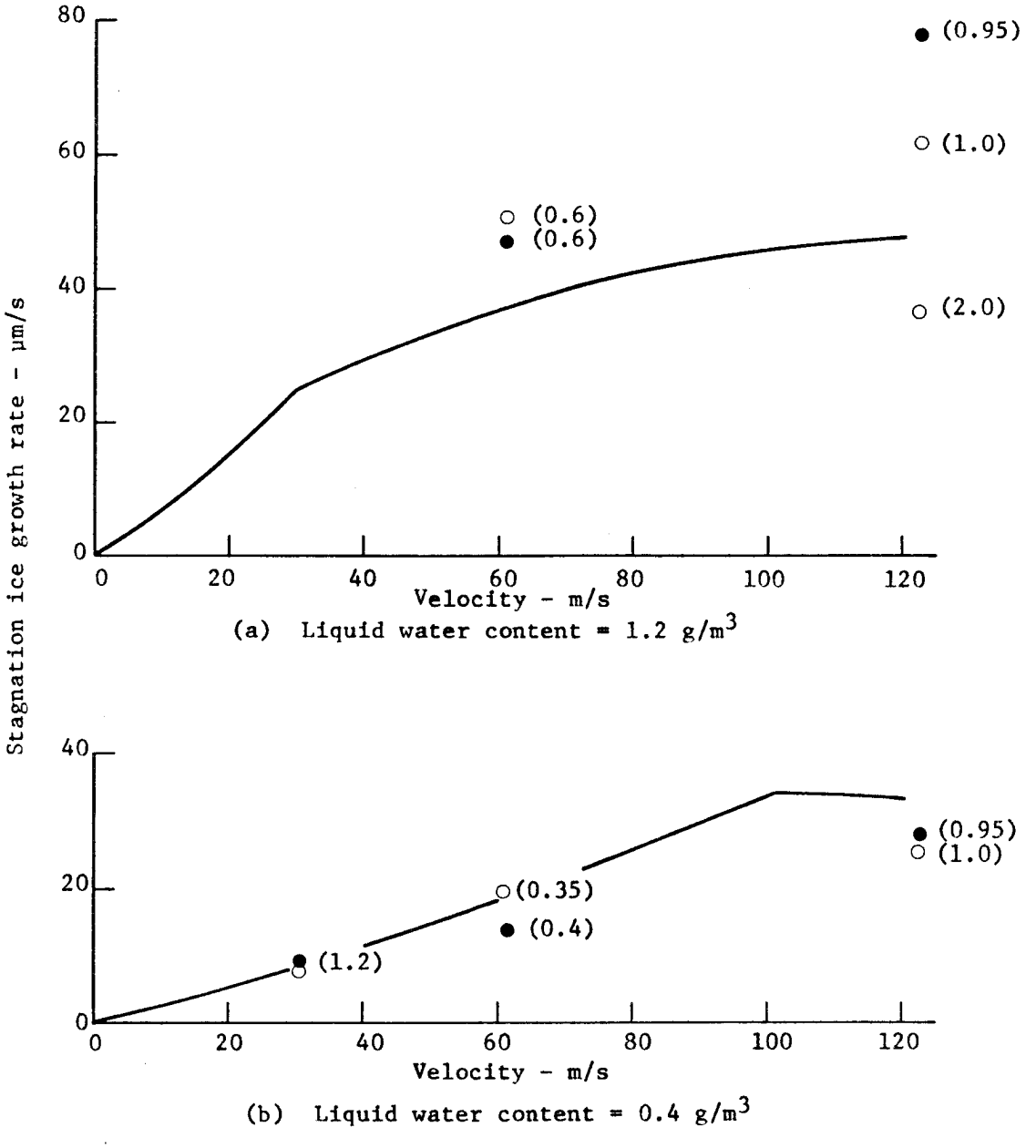

FIG. 17 STAGNATION LINE ICING RATE IN MIXED CONDITIONS AT -15°C

Solid points are experimental values from these tests. Open points are from Ref. 1. Lines are icing model predictions for liquid only. Ice crystal content (g/m^3) shown in parentheses.

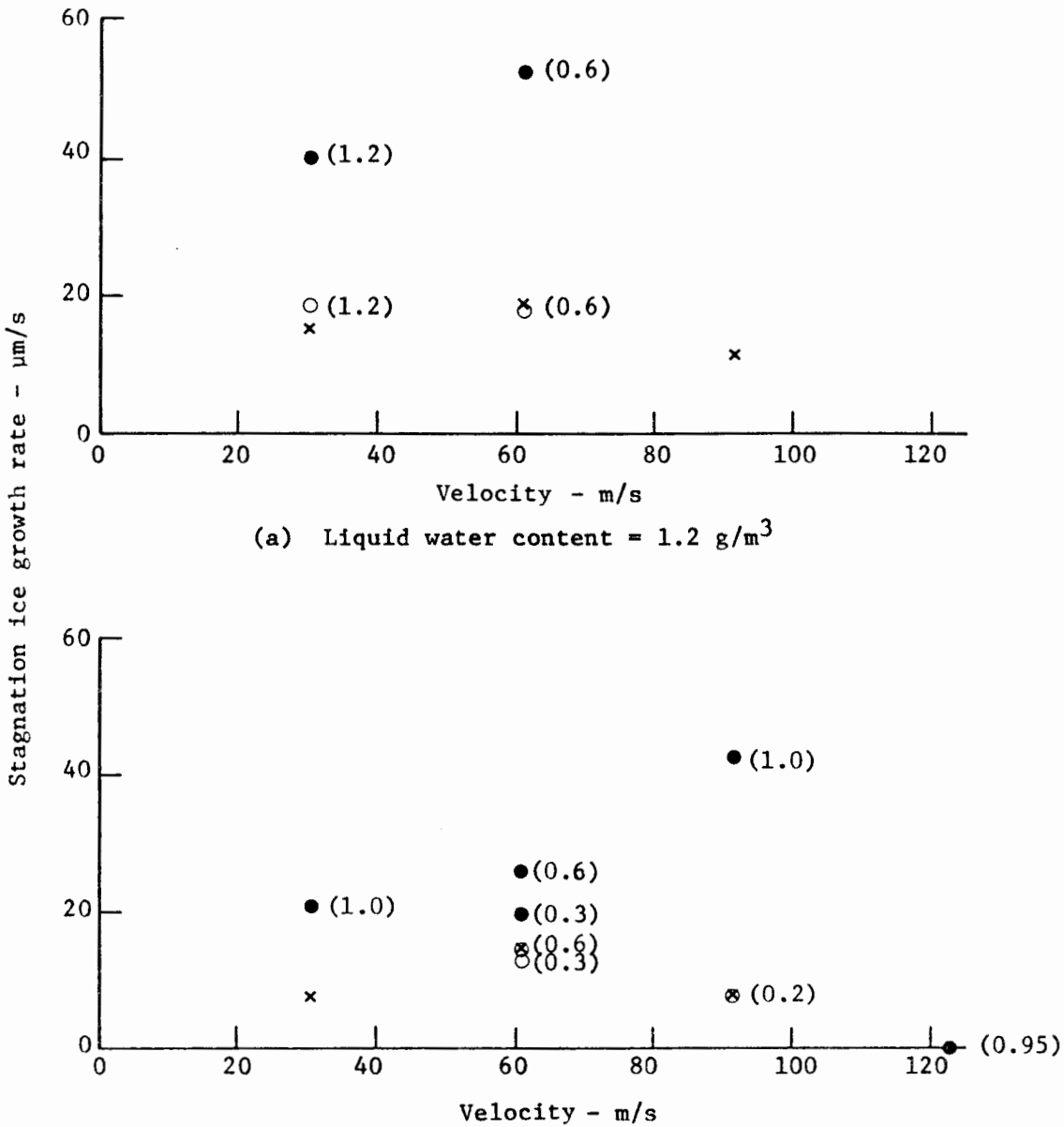

FIG. 18 STAGNATION LINE ICING RATE IN MIXED CONDITIONS AT -5°C

Solid points are experimental values from these tests, open points are from Ref. 1. Crosses are for liquid only from these tests.
Ice crystal content (g/m^3) shown in parentheses.

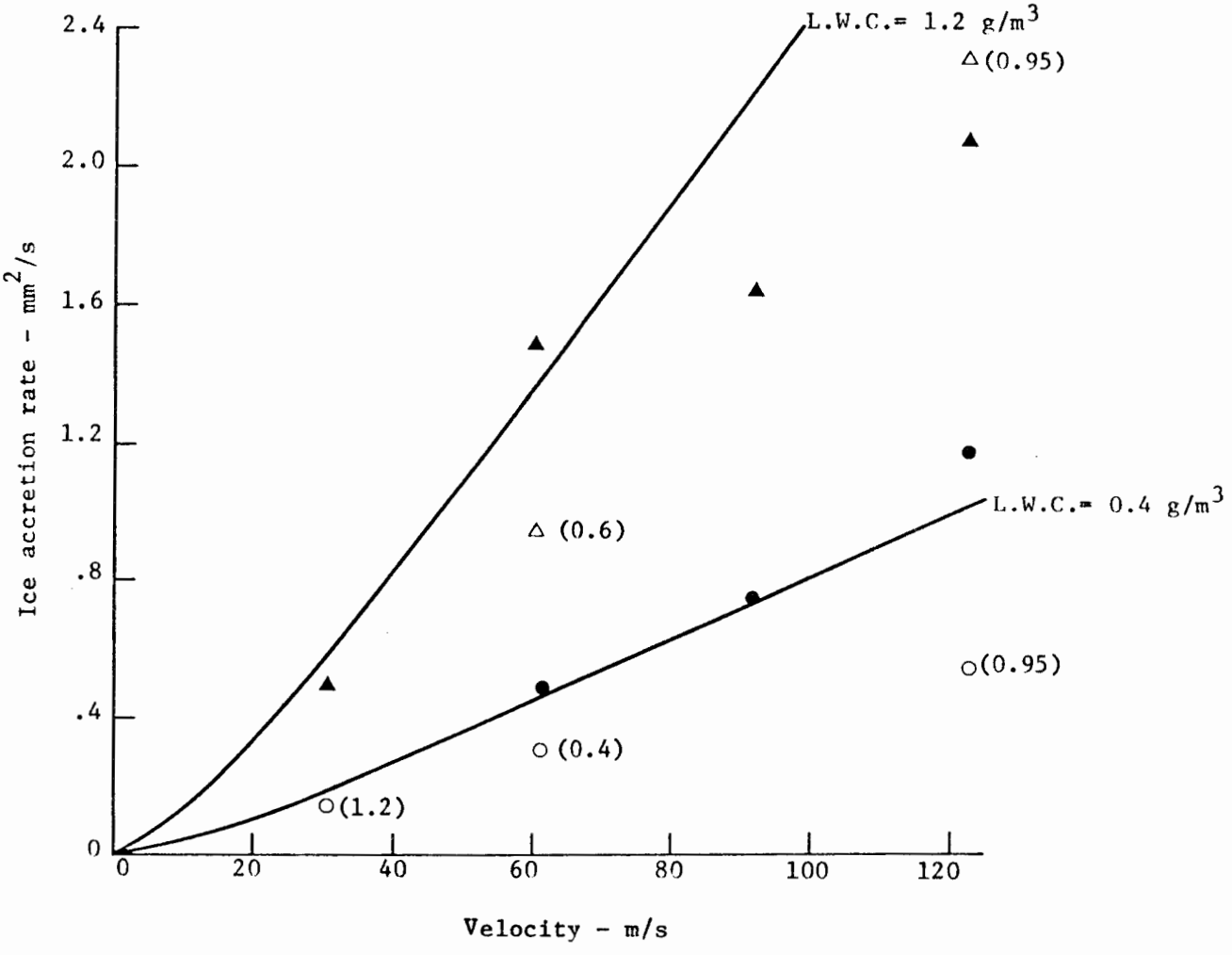

FIG. 19 CYLINDER ICE ACCRETION RATE AS A FUNCTION OF VELOCITY AT A TEMPERATURE OF -15°C

Solid circles are for liquid only at L.W.C. of 0.4 g/m^3. Open circles are for mixed conditions with L.W.C. of 0.4 g/m^3.

Solid triangles are for liquid only at L.W.C. of 1.2 g/m^3. Open triangles are for mixed conditions with L.W.C. of 1.2 g/m^3.

Ice crystal content (g/m^3) shown in parentheses.

Lines are calculated liquid only accretion rates assuming complete freezing.

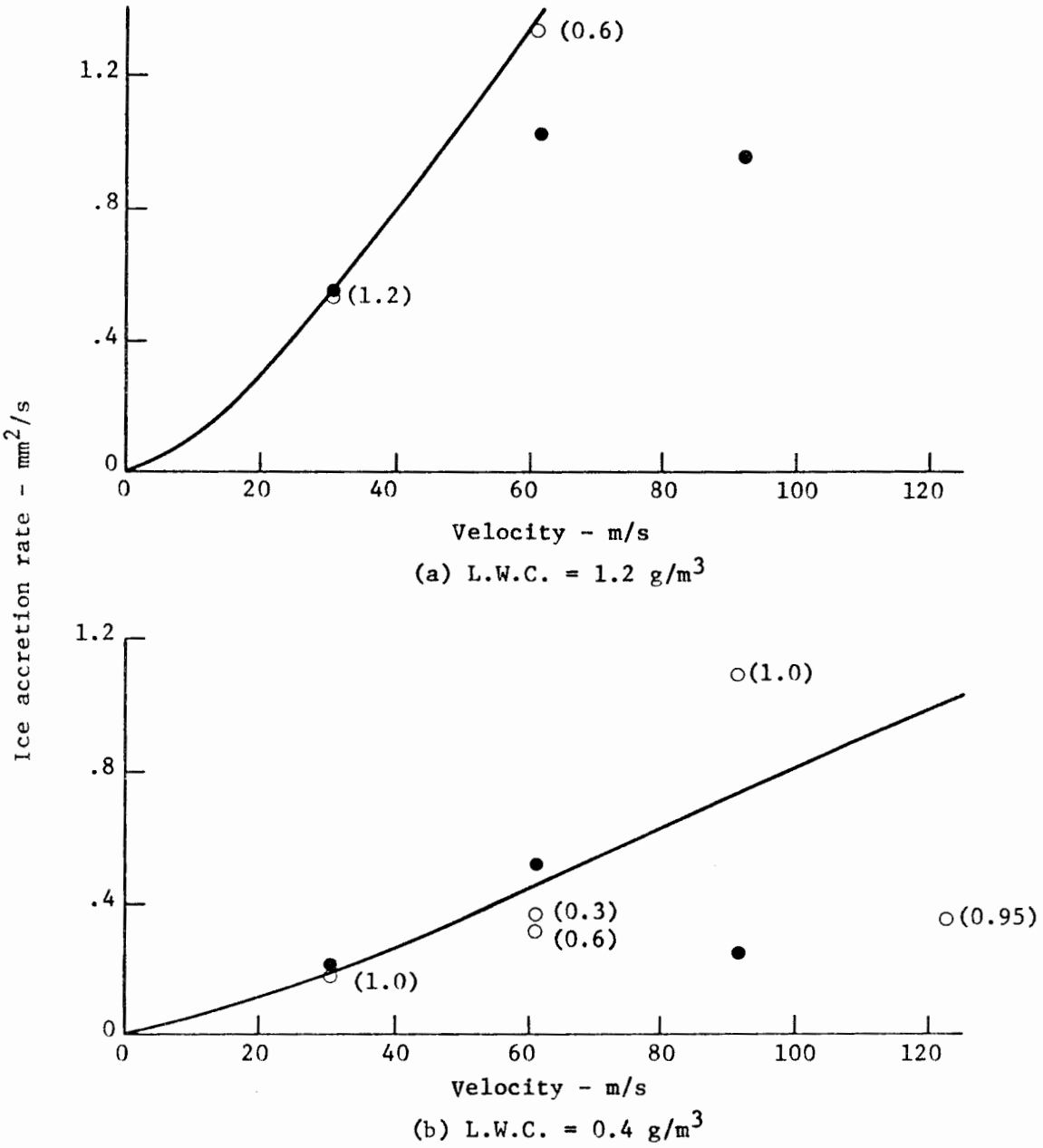

FIG. 20 CYLINDER ICE ACCRETION RATE AS A FUNCTION OF VELOCITY AT A TEMPERATURE OF -5°C

Solid circles are for liquid only.
Open circles are for mixed conditions.

Ice crystal content (g/m^3) shown in parentheses.

Lines are calculated liquid only accretion rates assuming complete freezing.

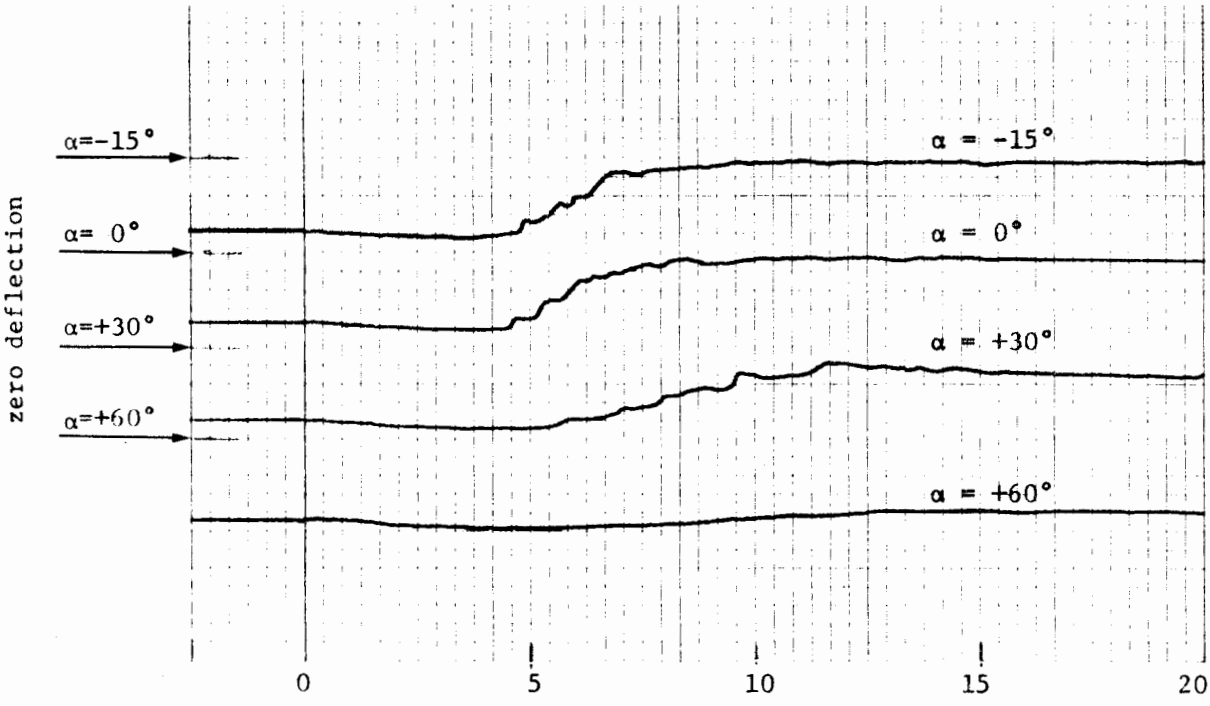

(a) Test #36, I.C.C. = 0

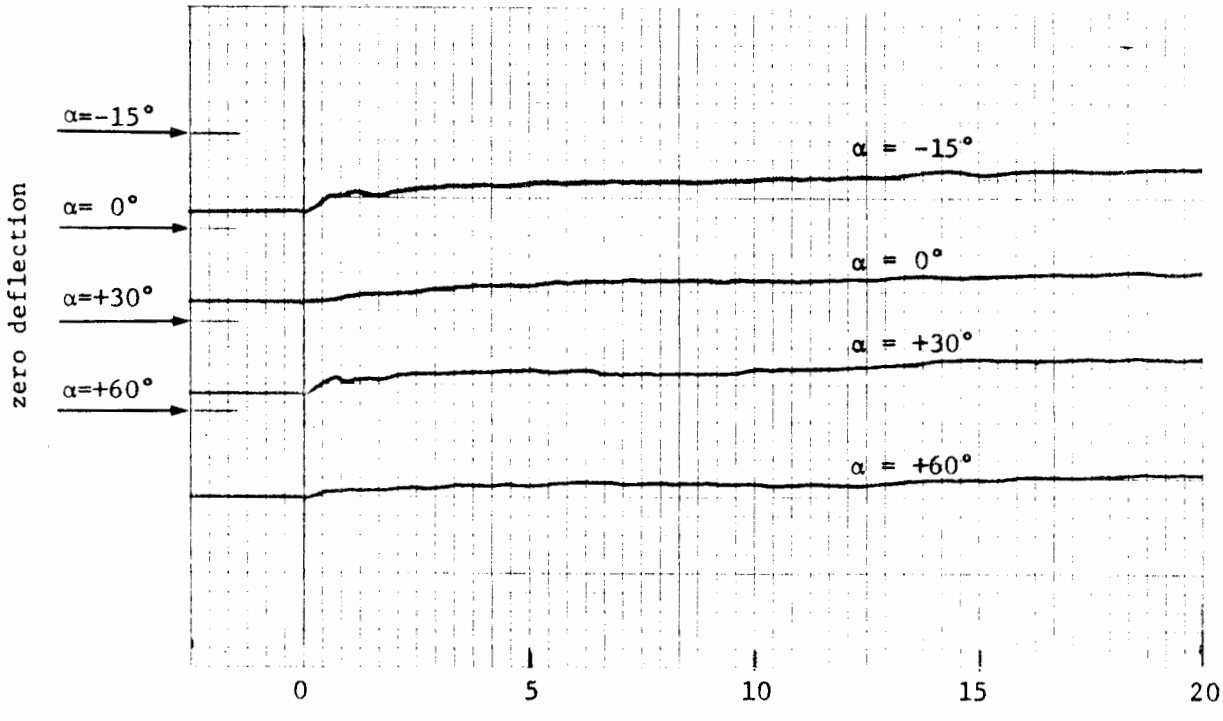

(b) Test #37, I.C.C. = 1.0 g/m^3

FIG. 21 CYLINDER SURFACE TEMPERATURE HISTORIES FOR INITIAL 20 SECONDS OF TESTS 36 AND 37. AIR SPEED = 30.5 m/s, NOMINAL AIR TEMPERATURE = -5°C, L.W.C. = 0.4 g/m^3

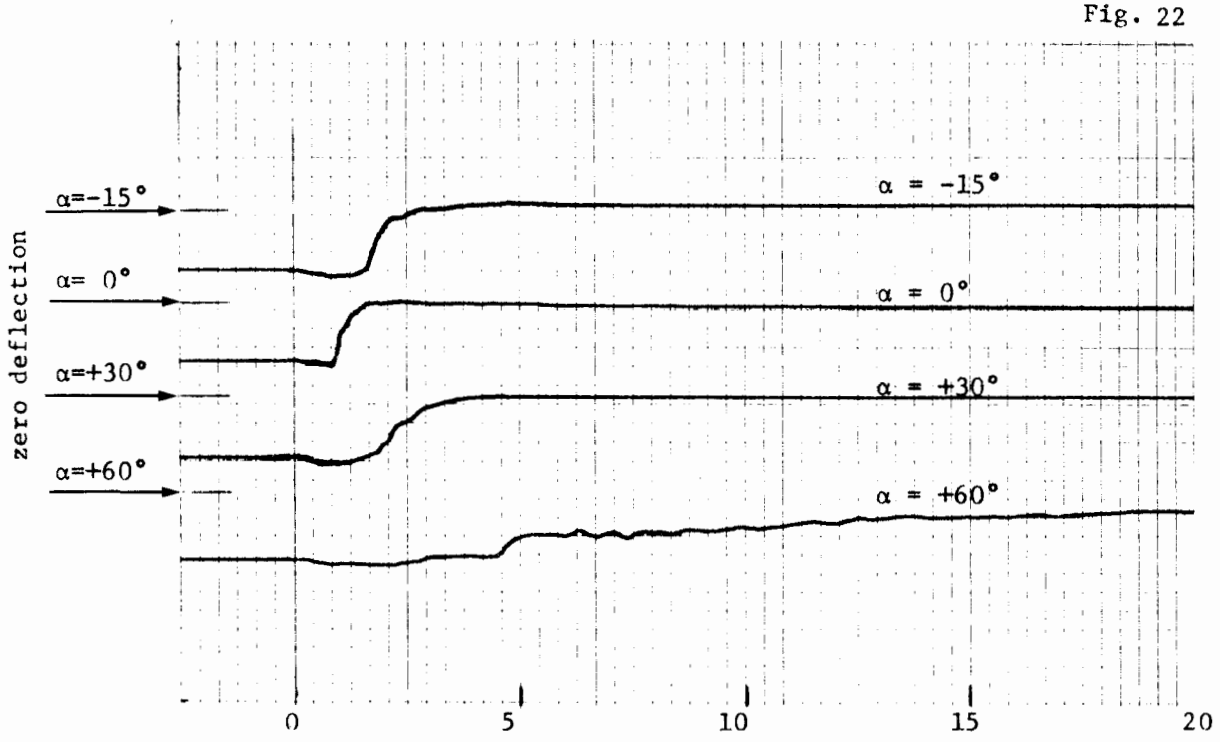

(a) Test #31, I.C.C. = 0

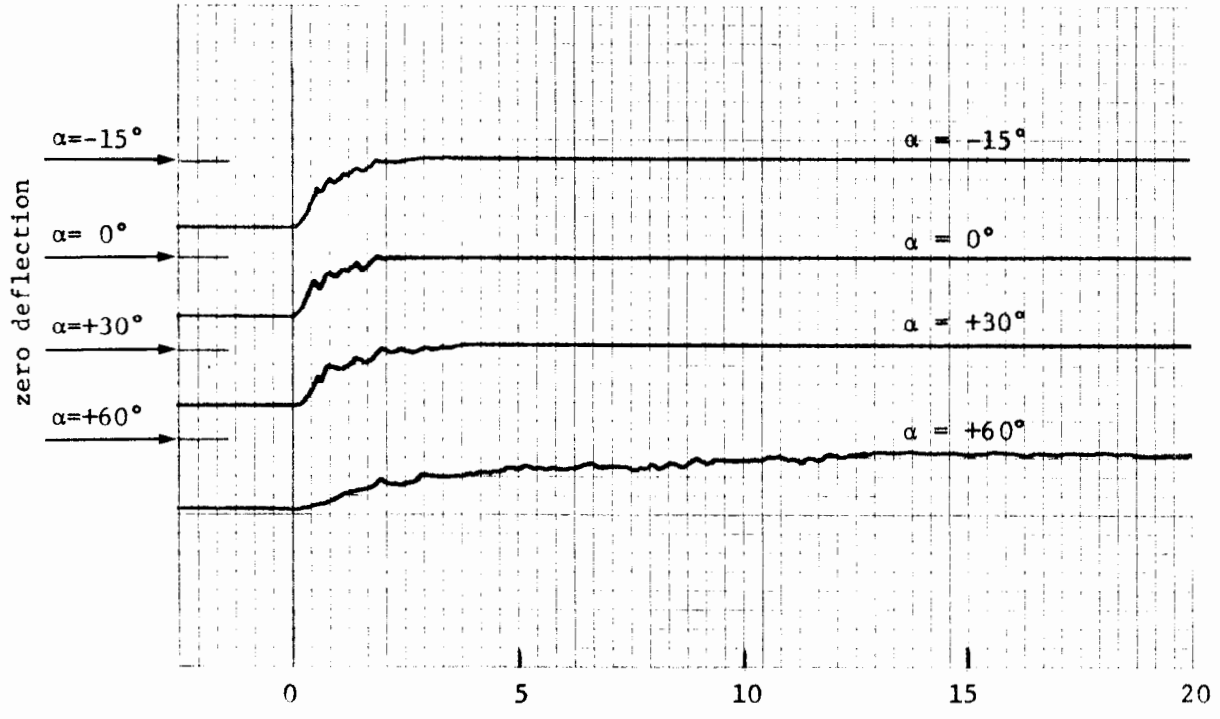

(b) Test #32, I.C.C. = 1.2 g/m^3

FIG. 22 CYLINDER SURFACE TEMPERATURE HISTORIES FOR INITIAL 20 SECONDS OF TESTS 31 AND 32. AIR SPEED = 30.5 m/s, NOMINAL AIR TEMPERATURE = -5°C, L.W.C. = 1.18 g/m^3

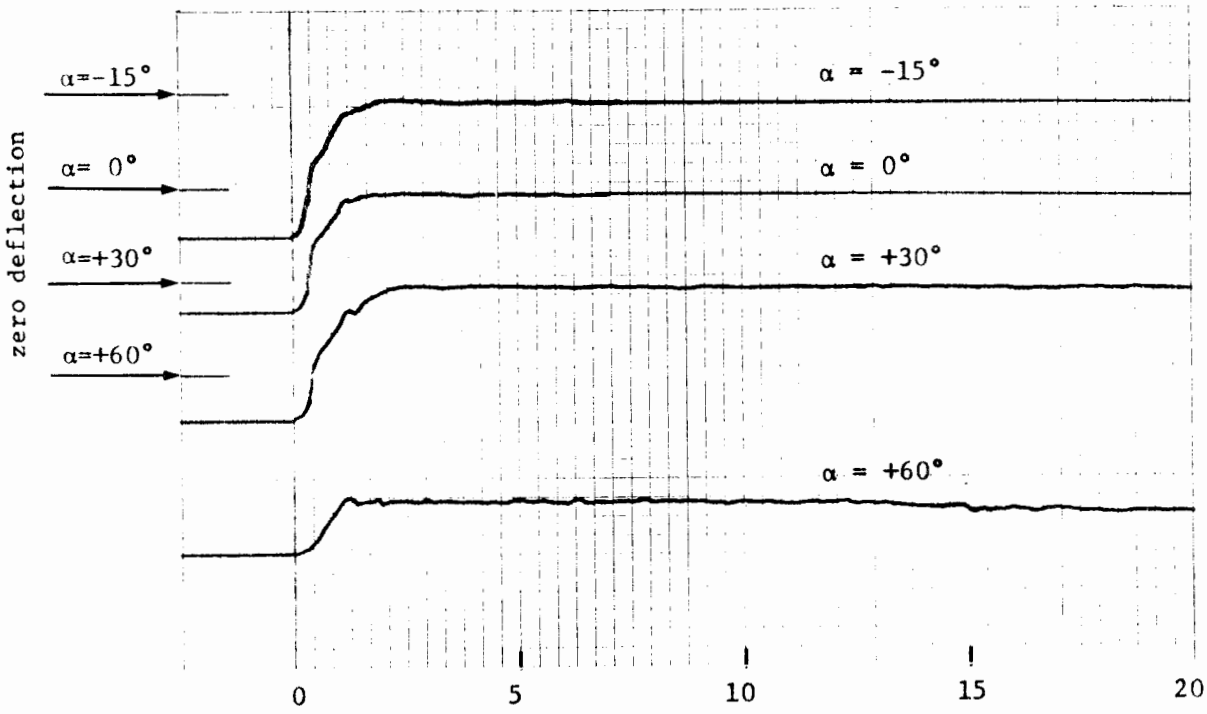

(a) Test #25, I.C.C. = 0

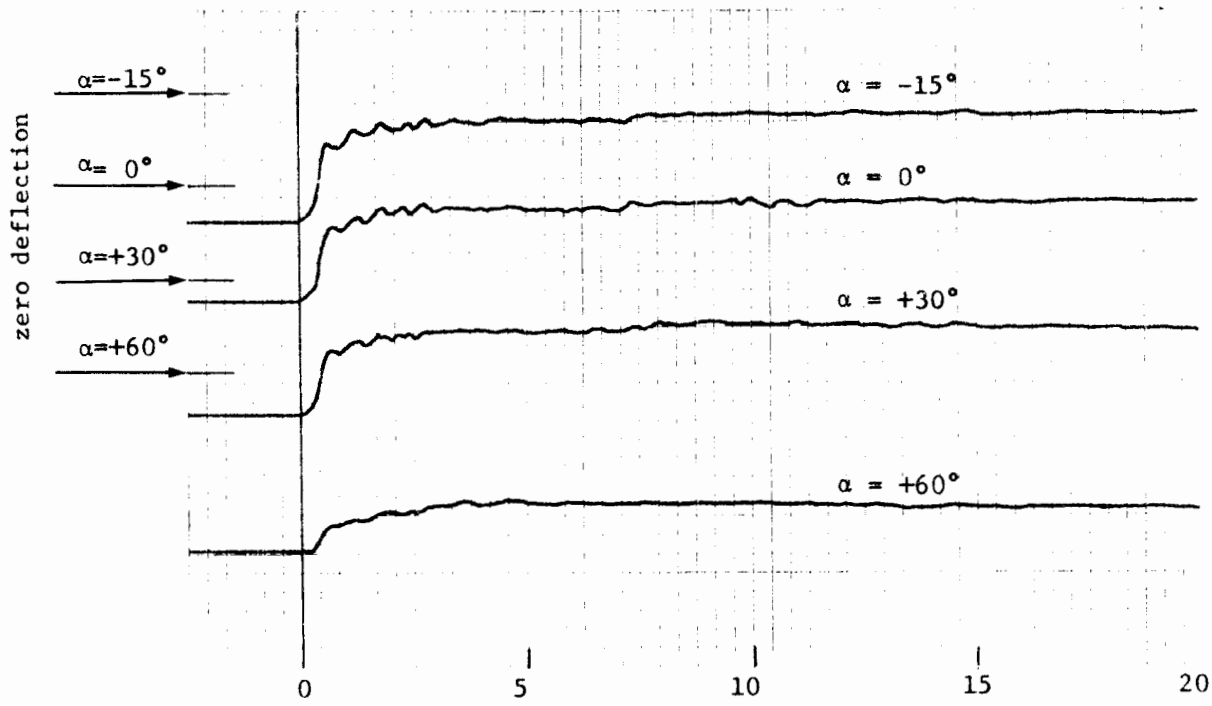

(b) Test #26, I.C.C. = 0.95 g/m^3

FIG. 23 CYLINDER SURFACE TEMPERATURE HISTORIES FOR INITIAL 20 SECONDS OF TESTS 25 AND 26. AIR SPEED = 122 m/s, NOMINAL AIR TEMPERATURE = -15°C, L.W.C. = 0.43 g/m^3

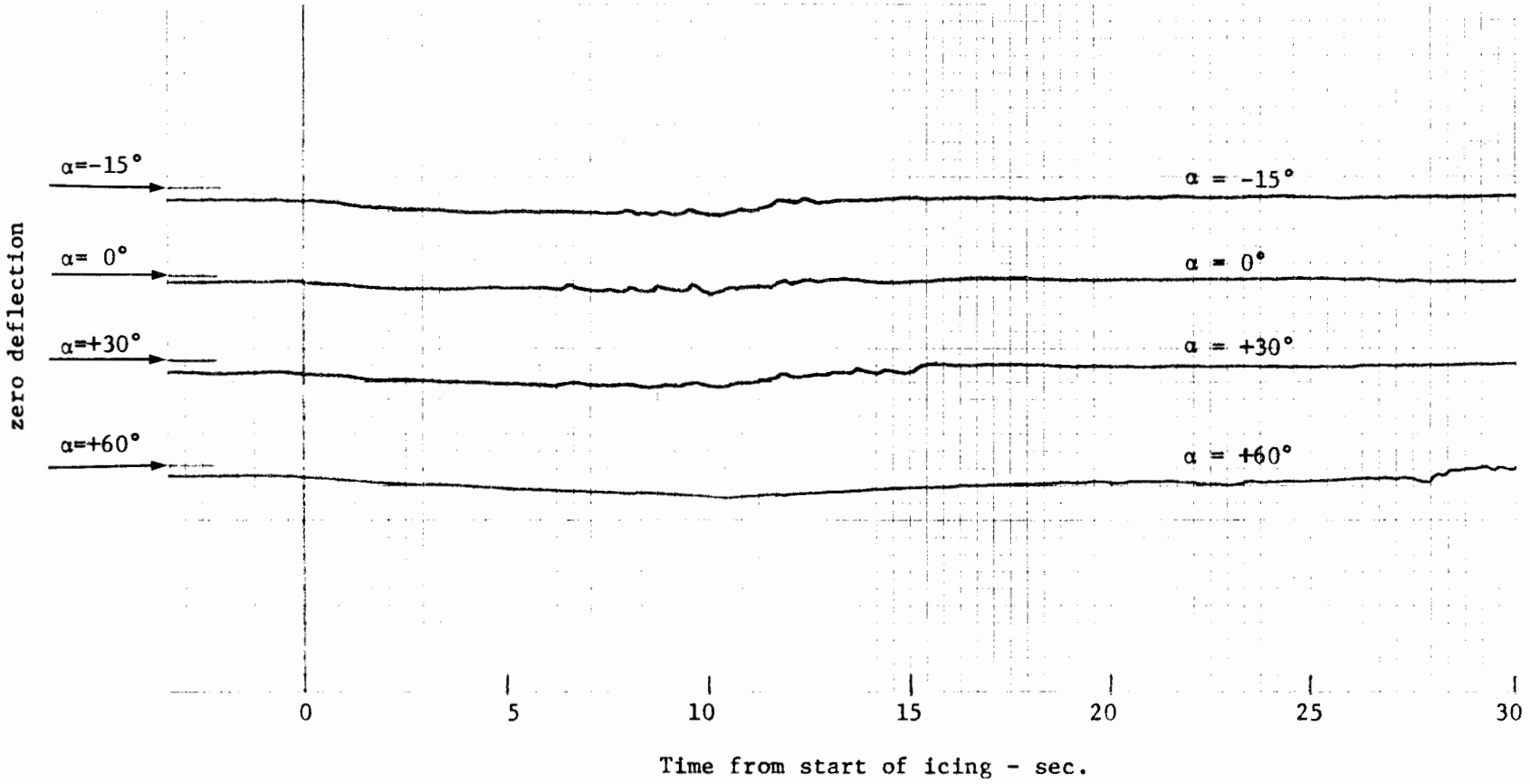

FIG. 24 CYLINDER SURFACE TEMPERATURE HISTORY FOR INITIAL 30 SECONDS OF TEST 21.
AIR SPEED = 91.5 m/s, NOMINAL AIR TEMPERATURE = -4.6°C,
L.W.C. = 0.4 g/m^3, I.C.C. = 0

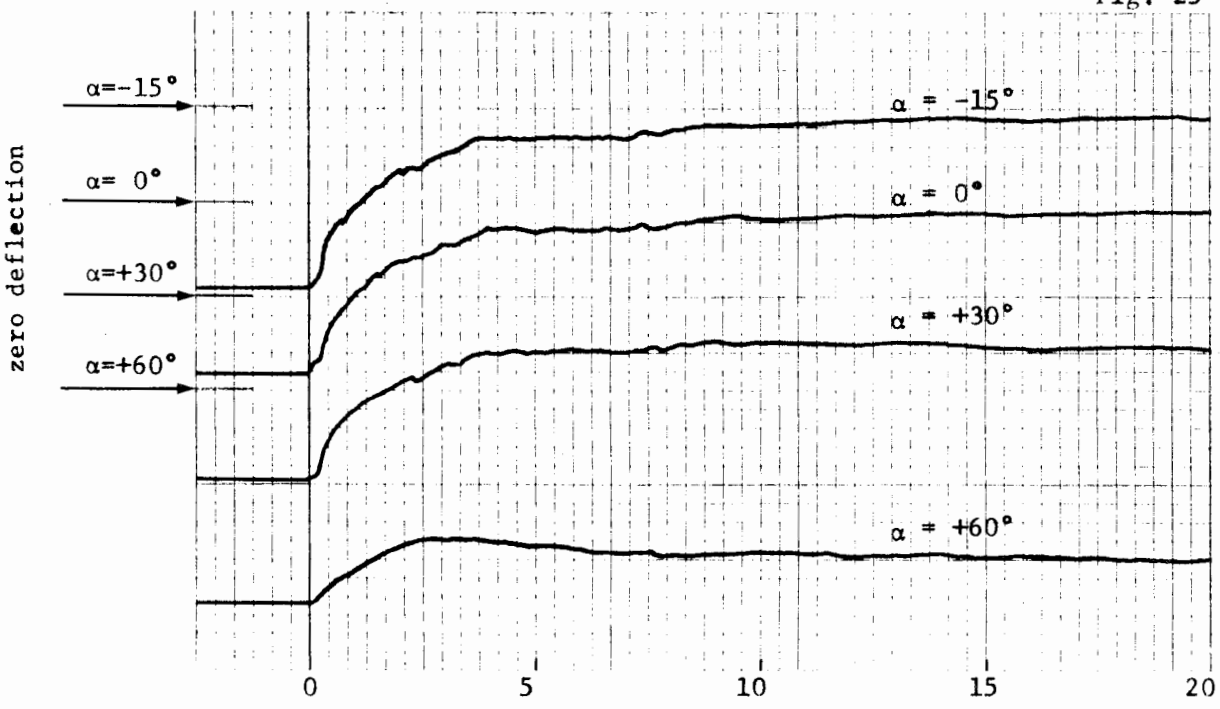

(a) Test #41, L.W.C.= 0.4 g/m^3

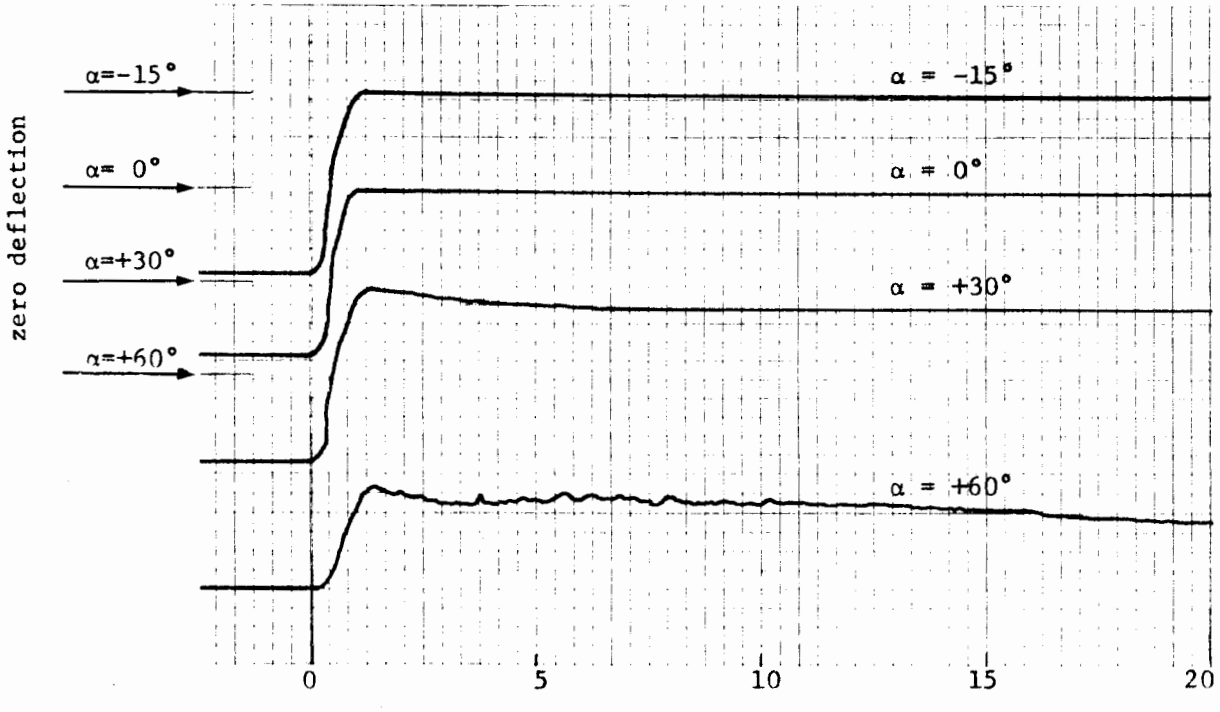

Time from start of icing - sec.

(b) Test #42, L.W.C. = 1.2 g/m^3

FIG. 25 CYLINDER SURFACE TEMPERATURE HISTORIES FOR INITIAL 20 SECONDS OF TESTS 41 AND 42. AIR SPEED = 91.5 m/s, NOMINAL AIR TEMPERATURE = -15°C, LIQUID ONLY CONDITIONS

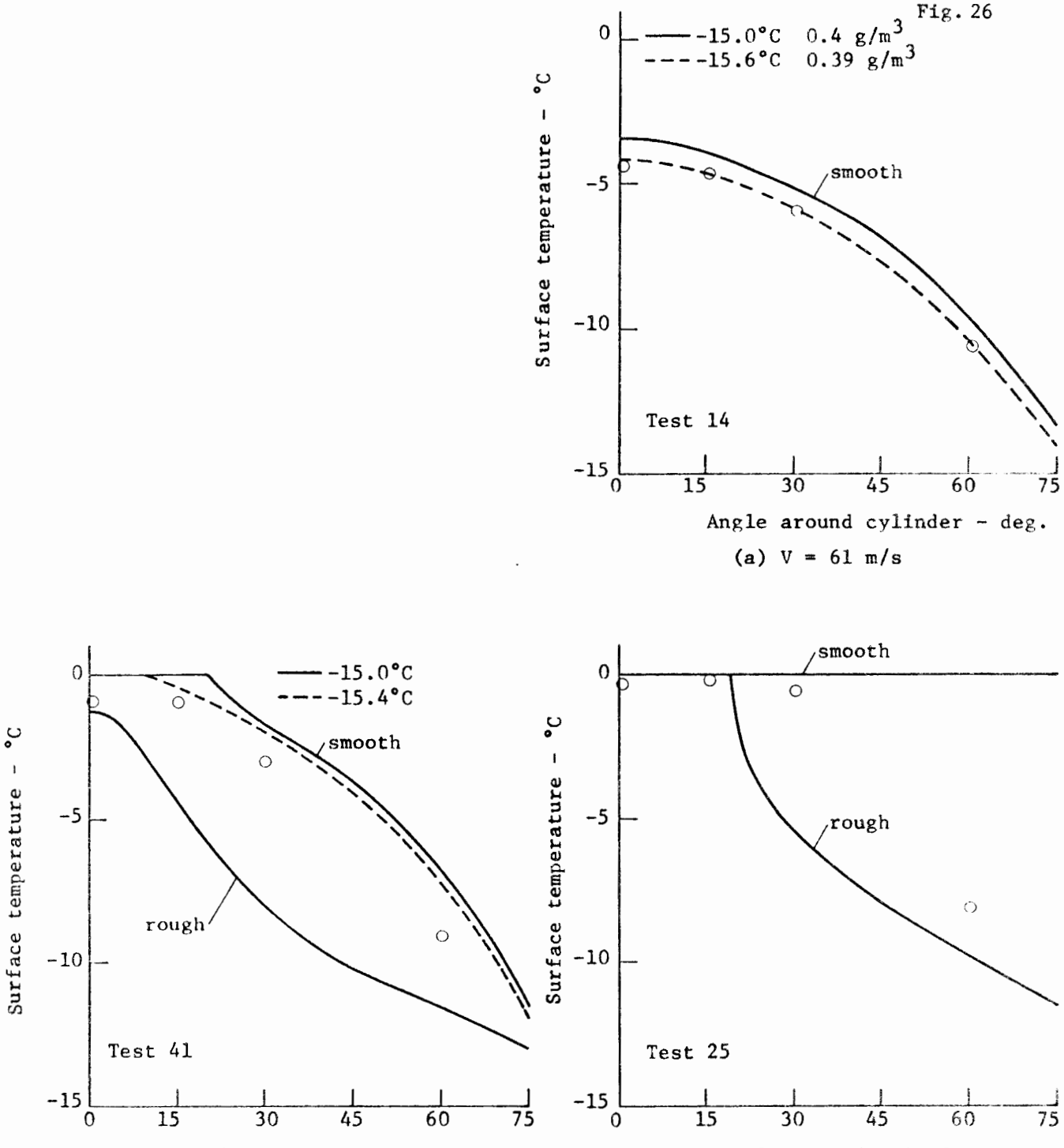

FIG. 26 EXPERIMENTAL AND MODEL-PREDICTED ICE SURFACE TEMPERATURES AROUND CYLINDER AT -15°C AIR TEMPERATURE WITH 0.4 g/m^3 LIQUID WATER ONLY

Points are experimental results, lines are model predictions.

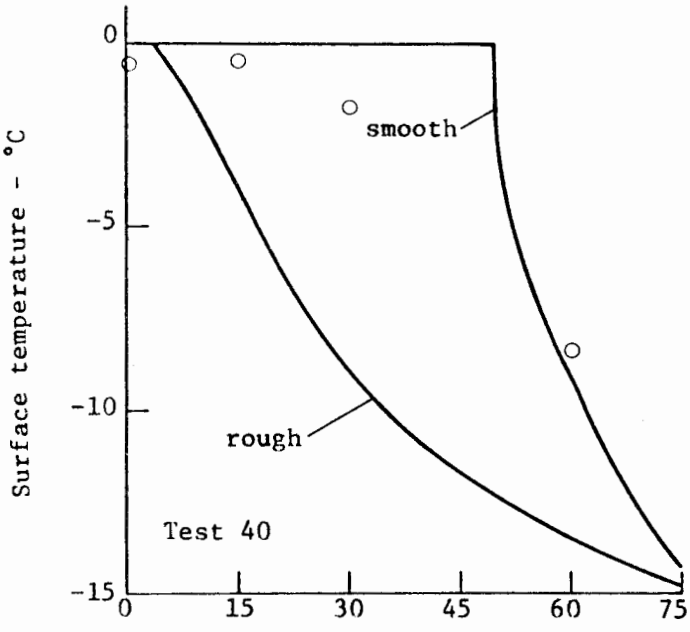

(a) V = 30.5 m/s

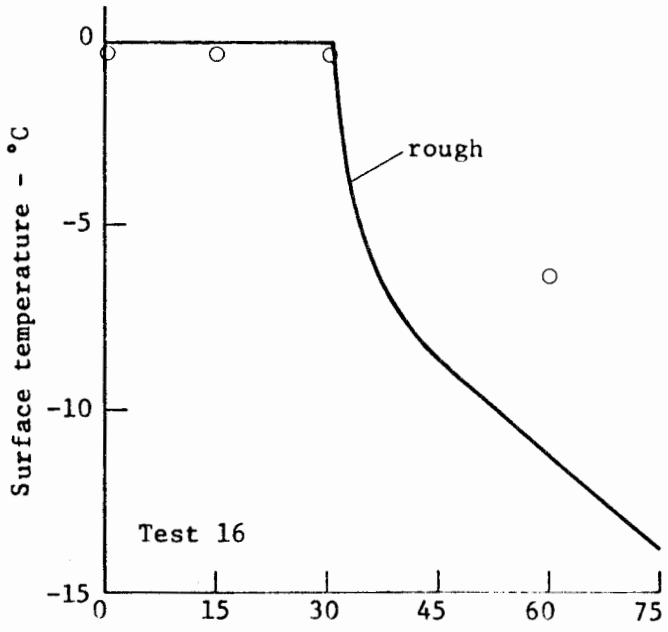

(b) V = 61 m/s

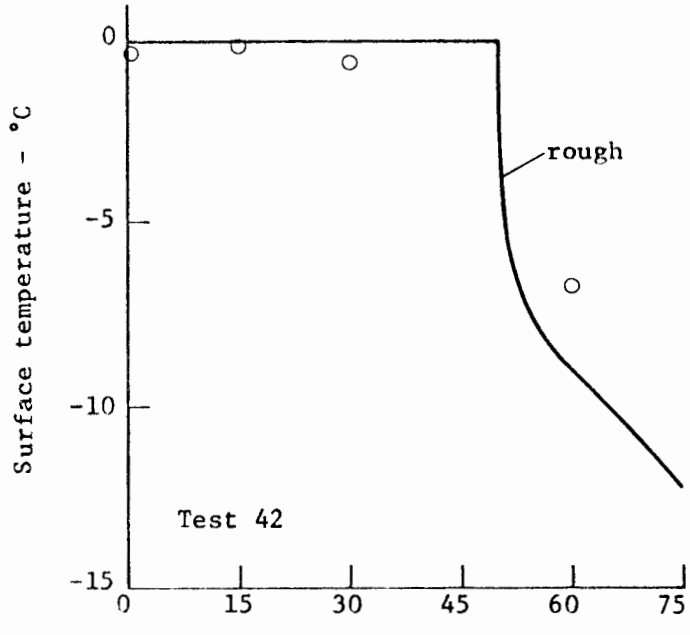

(c) V = 91.5 m/s

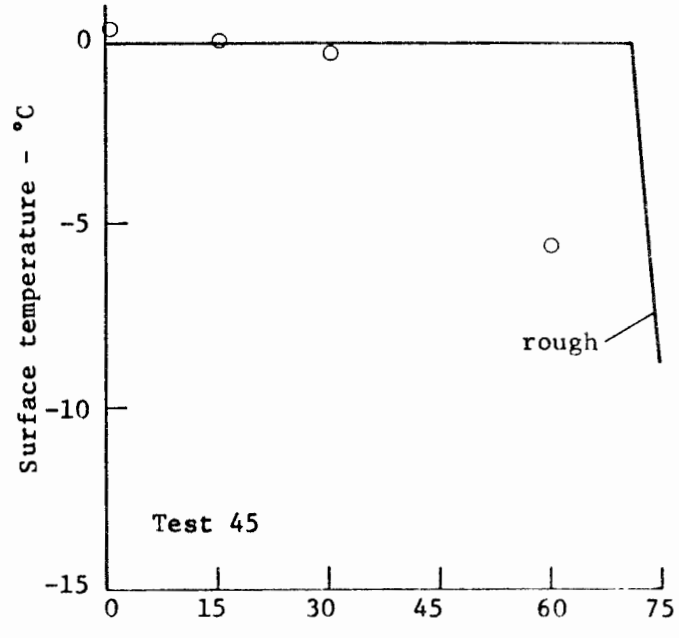

(d) V = 122 m/s

FIG. 27 EXPERIMENTAL AND MODEL-PREDICTED ICE SURFACE TEMPERATURES AROUND CYLINDER AT -15°C AIR TEMPERATURE WITH 1.2 g/m^3 LIQUID WATER ONLY

Points are experimental results, lines are model predictions.

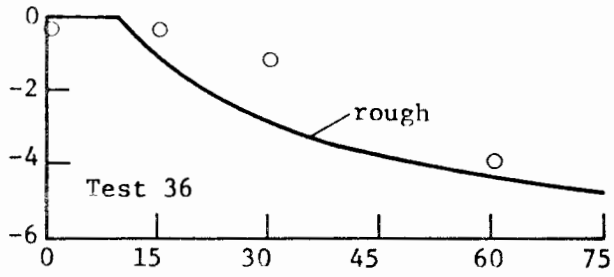

Angle around cylinder - deg.

(a) V = 30.5 m/s
L.W.C. = 0.4 g/m^3

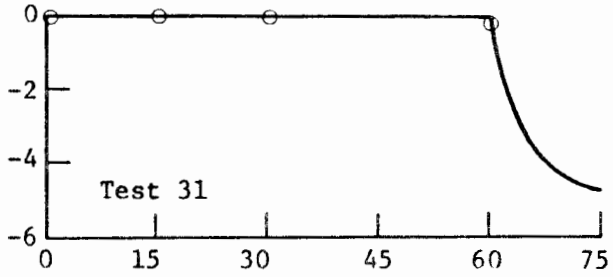

Angle around cylinder - deg.

(d) V = 30.5 m/s
L.W.C. = 1.2 g/m^3

Surface temperature - °C

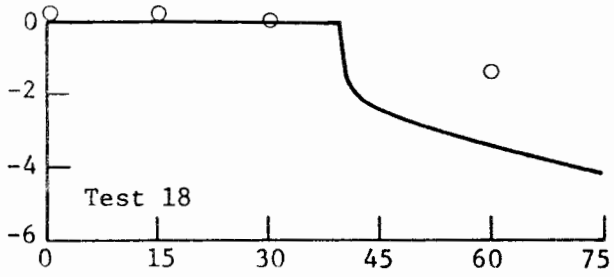

Angle around cylinder - deg.

(b) V = 61 m/s
L.W.C. = 0.4 g/m^3

Surface temperature - °C

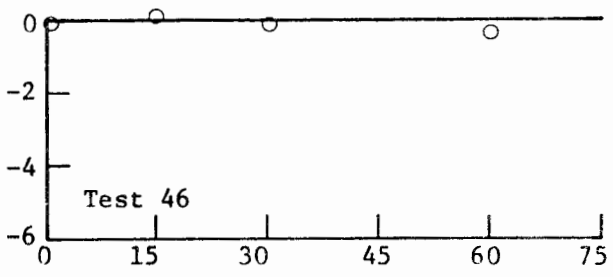

Angle around cylinder - deg.

(e) V = 61 m/s
L.W.C. = 1.2 g/m^3

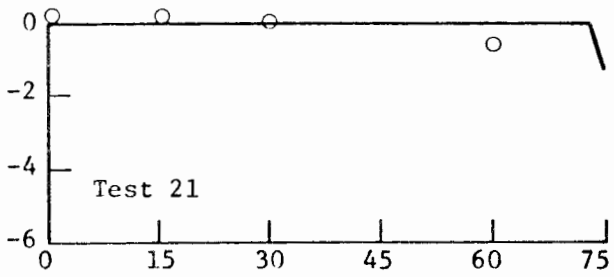

Angle around cylinder - deg.

(c) V = 91.5 m/s
L.W.C. = 0.4 g/m^3

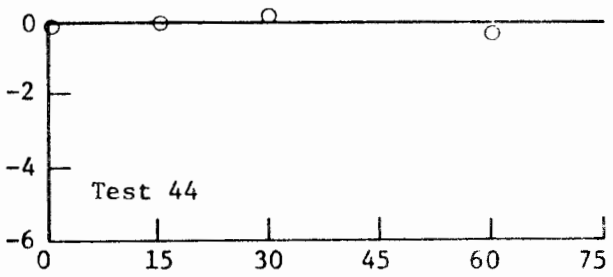

Angle around cylinder - deg.

(f) V = 91.5 m/s
L.W.C. = 1.2 g/m^3

FIG. 28 EXPERIMENTAL AND MODEL-PREDICTED ICE SURFACE TEMPERATURES AROUND CYLINDER AT -5°C AIR TEMPERATURE WITH LIQUID WATER ONLY

Points are experimental results, lines are model predictions.

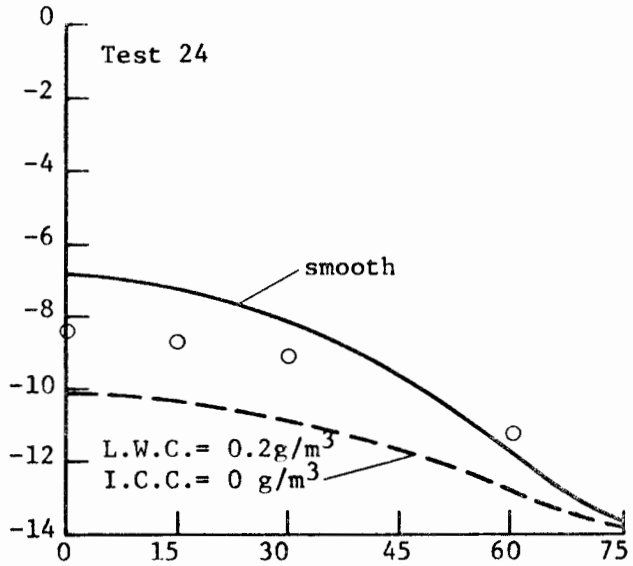

Angle around cylinder - deg.

(a) V = 30.5 m/s L.W.C. = 0.40 g/m^3
I.C.C. = 1.2 g/m^3

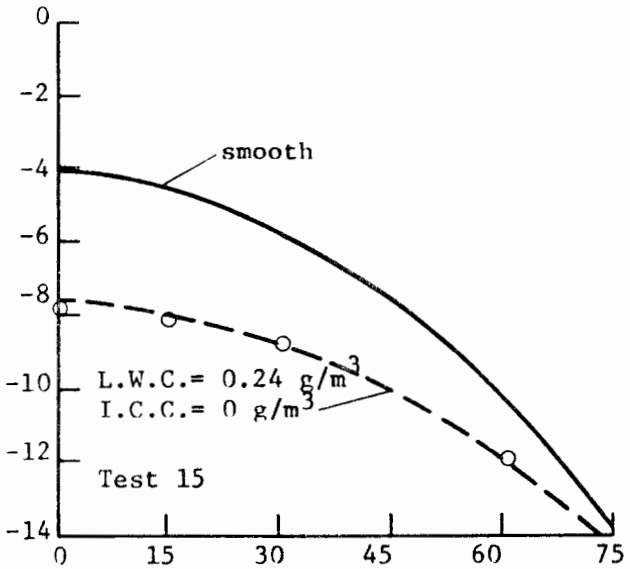

Angle around cylinder - deg.

(b) V = 61 m/s L.W.C. = 0.39 g/m^3
I.C.C. = 0.4 g/m^3

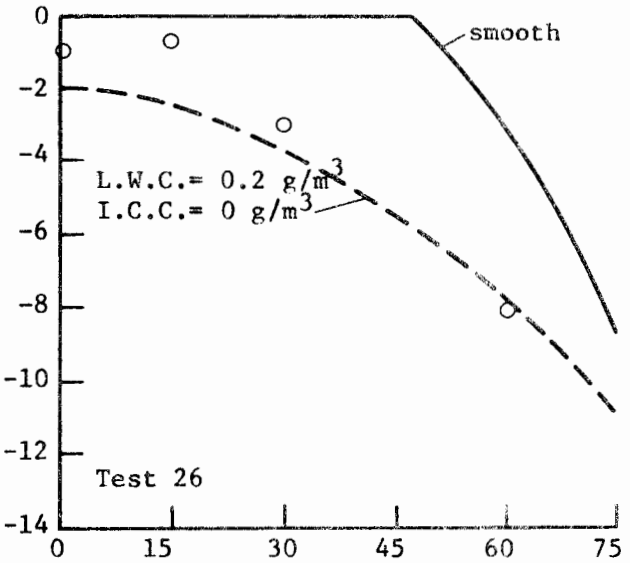

Angle around cylinder - deg.

(c) V = 122 m/s L.W.C. = 0.43 g/m^3
I.C.C. = 0.95 g/m^3

FIG. 29 EXPERIMENTAL AND MODEL-PREDICTED ICE SURFACE TEMPERATURES AROUND CYLINDER AT -15°C AIR TEMPERATURE UNDER MIXED CONDITIONS WITH L.W.C. = 0.4 g/m^3

Points are experimental results, lines are model predictions.

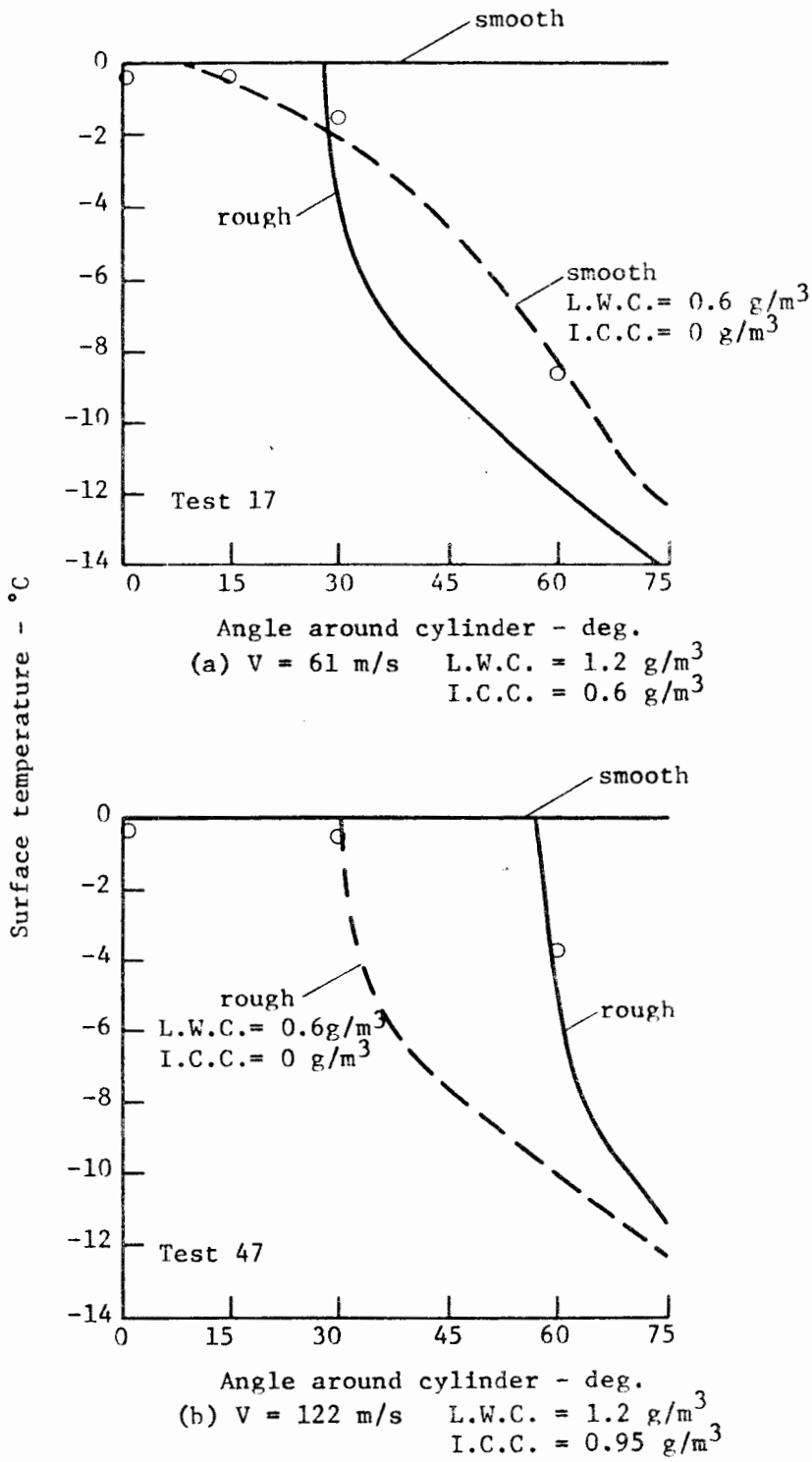

FIG. 30 EXPERIMENTAL AND MODEL-PREDICTED ICE SURFACE TEMPERATURES AROUND CYLINDER AT -15°C AIR TEMPERATURE UNDER MIXED CONDITIONS WITH L.W.C. = 1.2 g/m^3

Points are experimental results, lines are model predictions.

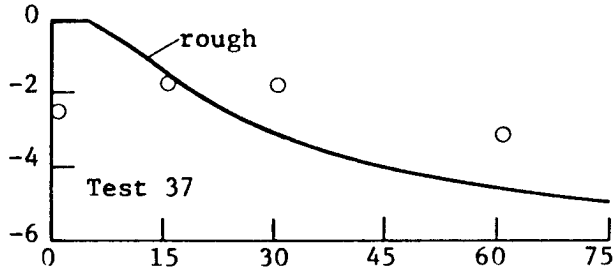

Angle around cylinder - deg.

(a) V = 30.5 m/s L.W.C. = 0.40 g/m^3
I.C.C. = 1.0 g/m^3

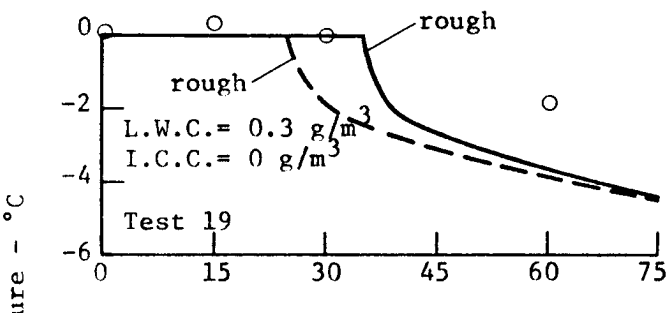

Angle around cylinder - deg.

(b) V = 61 m/s L.W.C. = 0.39 g/m^3
I.C.C. = 0.30 g/m^3

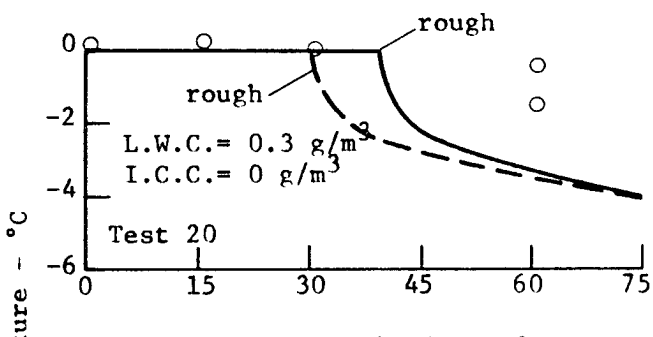

Angle around cylinder - deg.

(c) V = 61 m/s L.W.C. = 0.39 g/m^3
I.C.C. = 0.60 g/m^3

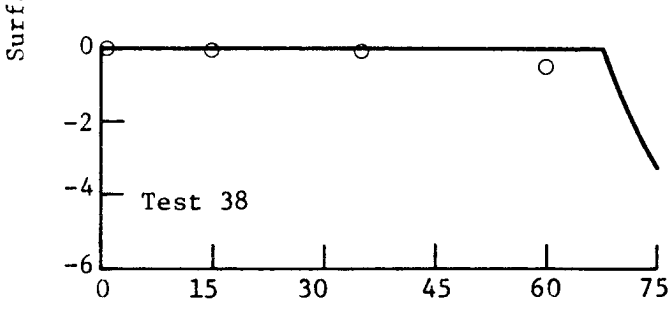

Angle around cylinder - deg.

(d) V = 91.5 m/s L.W.C. = 0.40 g/m^3
I.C.C. = 1.0 g/m^3

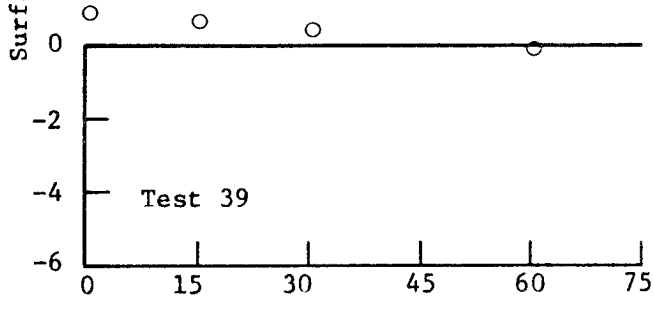

Angle around cylinder - deg.

(e) V = 122 m/s L.W.C. = 0.38 g/m^3
I.C.C. = 0.95 g/m^3

FIG. 31 EXPERIMENTAL AND MODEL-PREDICTED ICE SURFACE TEMPERATURES AROUND CYLINDER AT -5°C AIR TEMPERATURE UNDER MIXED CONDITIONS WITH L.W.C. = 0.4 g/m^3

Points are experimental results, lines are model predictions.

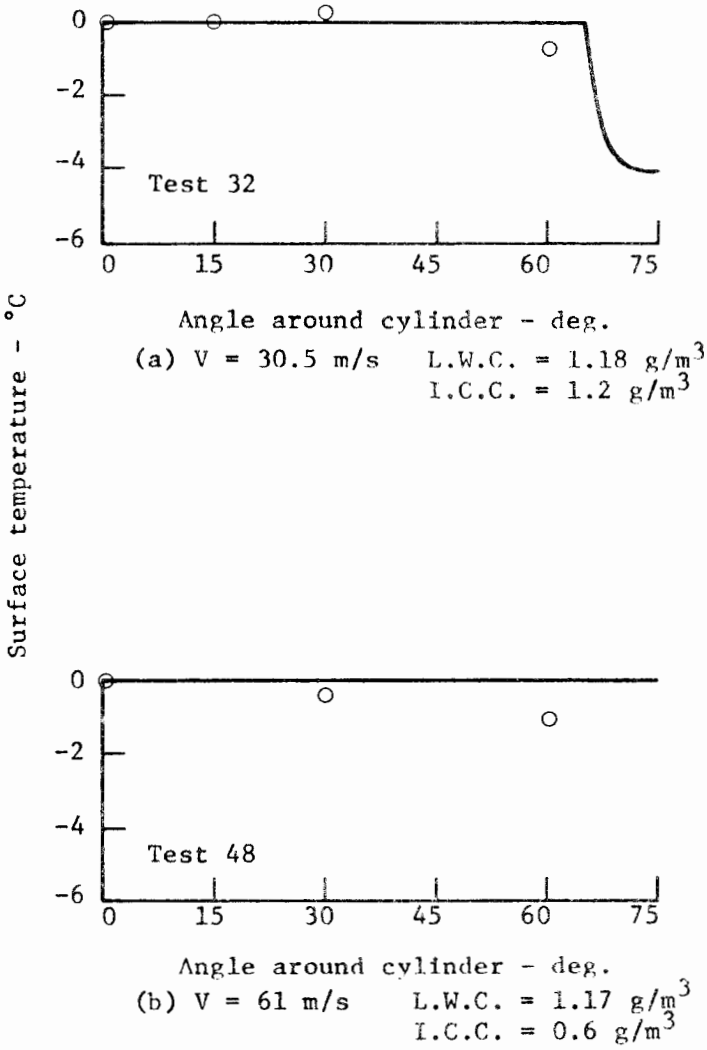

FIG. 32 EXPERIMENTAL AND MODEL-PREDICTED ICE SURFACE TEMPERATURE AROUND CYLINDER AT -5°C AIR TEMPERATURE UNDER MIXED CONDITIONS WITH L.W.C. = 1.2 g/m^3

Points are experimental results, lines are model predictions.